

MICROSTRUCTURAL RESPONSE OF  
ALUMINUM-MAGNESIUM ALLOYS TO  
THERMOMECHANICAL PROCESSING.

Charles Pierson Bingay



# NAVAL POSTGRADUATE SCHOOL

Monterey, California



## THESIS

MICROSTRUCTURAL RESPONSE OF ALUMINUM-  
MAGNESIUM ALLOYS TO  
THERMOMECHANICAL PROCESSING

by

Charles Pierson Bingay

December 1977

Thesis Advisor:

T. R. McNelley

Approved for public release; distribution unlimited.

T181446





REPORT DOCUMENTATION PAGE		READ INSTRUCTIONS BEFORE COMPLETING FORM
1. REPORT NUMBER	2. GOVT ACCESSION NO.	3. RECIPIENT'S CATALOG NUMBER
4. TITLE (and Subtitle) Microstructural Response of Aluminum-Magnesium Alloys to Thermomechanical Processing		5. TYPE OF REPORT & PERIOD COVERED Master's Thesis; December 1977
		6. PERFORMING ORG. REPORT NUMBER
7. AUTHOR(s) Charles Person Bingay		8. CONTRACT OR GRANT NUMBER(s)
9. PERFORMING ORGANIZATION NAME AND ADDRESS Naval Postgraduate School Monterey, California 93940		10. PROGRAM ELEMENT, PROJECT, TASK AREA & WORK UNIT NUMBERS
11. CONTROLLING OFFICE NAME AND ADDRESS Naval Postgraduate School Monterey, California 93940		12. REPORT DATE December 1977
		13. NUMBER OF PAGES 100
14. MONITORING AGENCY NAME & ADDRESS (if different from Controlling Office) Naval Postgraduate School Monterey, California 93940		15. SECURITY CLASS. (of this report)
		15a. DECLASSIFICATION/DOWNGRADING SCHEDULE
16. DISTRIBUTION STATEMENT (of this Report)  Approved for public release; distribution unlimited.		
17. DISTRIBUTION STATEMENT (of the abstract entered in Block 20, if different from Report)		
18. SUPPLEMENTARY NOTES		
19. KEY WORDS (Continue on reverse side if necessary and identify by block number) Aluminum Alloys Aluminum-Magnesium Alloys Thermomechanical Processing		
20. ABSTRACT (Continue on reverse side if necessary and identify by block number)  Mechanisms of microstructural refinement in aluminum-magnesium alloys were investigated. Alloys containing from 15% to 19% magnesium were exposed to various processing schemes, and the resulting microstructures were examined. Isothermal forging resulted in some refinement depending on the temperature, strain and strain rate. However, all samples isothermally forged		



exhibited microstructures having relatively large amounts of the brittle intermetallic phase present. The addition of tertiary alloy elements resulted in little improvement in microstructure. Non-isothermal schemes resulted in the most promising microstructures. A process of high temperature soaking followed by deformation at relatively lower temperatures is concluded to be the most promising means for processing alloys with magnesium contents below 15% by weight.



Approved for public release; distribution unlimited.

Microstructural Response of Aluminum-  
Magnesium Alloys to Thermomechanical Processing

by

Charles Pierson Bingay  
Lieutenant, United States Navy  
B.A., University of Washington, 1969

Submitted in partial fulfillment of the  
requirements for the degree of

MASTER OF SCIENCE IN APPLIED SCIENCE

from the

NAVAL POSTGRADUATE SCHOOL  
December 1977



## ABSTRACT

Mechanisms of microstructural refinement in aluminum-magnesium alloys were investigated. Alloys containing from 15% to 19% magnesium were exposed to various processing schemes, and the resulting microstructures were examined. Isothermal forging resulted in some refinement depending on the temperature, strain and strain rate. However, all samples isothermally forged exhibited microstructures having relatively large amounts of the brittle intermetallic phase present. The addition of tertiary alloy elements resulted in little improvement in microstructure. Non-isothermal schemes resulted in the most promising microstructures. A process of high temperature soaking followed by deformation at relatively lower temperatures is concluded to be the most promising means for processing alloys with magnesium contents below 15% by weight.





## TABLE OF CONTENTS

I.	INTRODUCTION -----	11
II.	BACKGROUND -----	13
	A. THE ALUMINUM-MAGNESIUM SYSTEM -----	13
	B. PREVIOUS RESEARCH -----	17
III.	GENERAL DISCUSSION OF RESEARCH -----	20
	A. OBJECTIVES AND PLAN OF INVESTIGATION -----	20
	B. MICROSCOPY PROCEDURES -----	21
	1. Mounting and Polishing -----	21
	2. Etching -----	22
	3. Observation Techniques -----	22
	C. SOURCE OF MATERIALS -----	23
IV.	ISOTHERMAL WORKING -----	25
	A. DISCUSSION -----	25
	B. EXPERIMENTAL PROCEDURES -----	27
	C. RESULTS OF ISOTHERMAL WORKING -----	28
V.	THE EFFECT OF HOT FORGING ON MICROSTRUCTURE -----	30
	A. DISCUSSION -----	30
	B. EXPERIMENTAL PROCEDURES -----	31
	C. RESULTS OF HOT FORGING -----	34
	1. Temperature Effects -----	35
	2. Strain Effects -----	36
	3. Strain Rate Effects -----	36
	4. Precipitation Structures -----	37
	D. DISCUSSION OF TEST RESULTS -----	37



VI.	THE EFFECT OF ALLOY CHEMISTRY -----	41
A.	CHEMICAL ANALYSIS -----	41
1.	Sample Selection -----	41
2.	Analysis Methods -----	41
a.	Atomic Absorption -----	41
b.	Emission Spectroscopy -----	43
3.	Results of Chemical Analysis -----	43
B.	EFFECTS OF ALLOY CHEMISTRY DURING FORGING ----	45
1.	Casting of Test Alloys -----	45
2.	Effects of Working on Test Alloys -----	46
VII.	THE EFFECTS OF NON-ISOTHERMAL TREATMENTS -----	48
A.	MATERIAL THERMAL RESPONSE CHARACTERISTICS ----	48
B.	THERMAL TREATMENT EFFECTS -----	50
1.	Experimental Procedures -----	50
2.	Results of Thermal Treatment -----	51
C.	THERMOMECHANICAL TREATMENT EFFECTS -----	52
1.	Experimental Procedures -----	53
2.	Thermomechanical Working Results -----	55
VIII.	SUMMARY AND DISCUSSION OF RESULTS -----	56
IX.	CONCLUSIONS AND RECOMMENDATIONS -----	61
	LIST OF TABLES -----	7
	LIST OF FIGURES -----	8
	LIST OF REFERENCES -----	99
	INITIAL DISTRIBUTION LIST -----	100



## LIST OF TABLES

I.	Test Conditions for Examination of the Effect of Strain, Strain Rate and Temperature on Microstructural Refinement -----	33
II.	Mean Free Path Data for the 19% Magnesium Alloy as a Function of Temperature and Strain Rate -----	38
III.	Alloy Compositions -----	44



## LIST OF FIGURES

1. Equilibrium phase diagram of the aluminum-magnesium binary system showing the aluminum rich portion to 36% magnesium by weight. -----	63
2. SEM photomicrograph showing the type of microstructure achieved by Ness in warm rolling of an Al-18Mg alloy. ----	64
3. SEM photomicrograph of a nominally Al-18Mg alloy showing final results of Ness' work. -----	65
4. Baldwin-Tate-Emery testing machine modified for hot forging operations. -----	66
5. SEM photomicrograph showing microstructure of Al-18Mg casting. -----	67
6. SEM photomicrograph of Al-18Mg alloy after isothermal forging at 400°C to a strain of 2.0. -----	68
7. SEM photomicrograph of Al-18Mg alloy after hot rolling 10% at 300°C. -----	69
8. Light photomicrograph of Al-18Mg alloy showing cracks in $\beta$ intermetallic particles as a result of deformation processing. -----	70
9. Instron testing machine modified for hot, isothermal compression testing. -----	71
10. Marshall split furnace opened to expose test chamber. ----	72
11. Light photomicrograph showing the cast structure of VEX0219-2 (Al-15Mg). -----	73
12. Light photomicrograph showing the cast structure of VEX0219-3 (Al-19Mg). -----	73
13. Light photomicrographs of VEX0219-2 (Al-15Mg) showing the effect of isothermal compression testing at various temperatures to a strain of 1.5 at a strain rate of $10^{-3} \text{ sec}^{-1}$ . 74	74
14. Compressive stress-strain curves for samples in Figure 13. 75	75
15. Light photomicrographs of VEX0219-3 (Al-19Mg) after isothermal compression testing at various temperatures to a strain of 1.5 at a strain rate of $10^{-3} \text{ sec}^{-1}$ . -----	76





16. Compressive stress-strain curves showing the relative flow stress levels of samples in Figures 15 and 17. -----	77
17. Light photomicrographs of VEX0219-3 (Al-19Mg) after isothermal compression testing at 270°C and a strain rate of $5 \times 10^{-3} \text{sec}^{-1}$ . -----	78
18. Light photomicrographs of VEX0219-3 (Al-19Mg) after isothermal compression testing at 415°C to a strain of 1.5 showing the effect of decreasing strain rate on microstructure. -----	79
19. Compressive stress-strain curves showing flow stress at various strain rates for samples of Figure 18. -----	80
20. SEM photomicrographs of VEX0219-3 (Al-19Mg) after isothermal compression testing at 200°C to a strain of 1.5 showing the $\beta$ precipitation structure resulting at three strain rates. -----	81
21. SEM photomicrographs of VEX0219-3 (Al-19Mg) after isothermal compression testing at 270°C to a strain of 1.5, showing the $\beta$ precipitation structure resulting at three strain rates. -----	82
22. SEM photomicrographs of VEX0219-3 (Al-19Mg) after isothermal compression testing at 415°C to a strain of 1.5, showing the $\beta$ precipitation structure resulting at three strain rates. -----	83
23. SEM photomicrographs of VEX0219-3 (Al-19Mg) before and after isothermal forging. -----	84
24. SEM photomicrographs of Al-17.8 Mg - 0.3Fe alloy before and after isothermal forging. -----	85
25. SEM photomicrographs of Al-18Mg-0.5Zn alloy before and after isothermal forging. -----	86
26. SEM photomicrographs of Al-19Mg-0.13Cu alloy before and after isothermal forging. -----	87
27. Temperature vs time curves for Al-Mg alloys. -----	88
28. SEM photomicrograph of VEX0219-3 (Al-19Mg) after being exposed to five temperature cycles, showing the overall microstructure. -----	89



29. SEM photomicrograph of VEX0219-3 (Al-19Mg) after being exposed to five temperature cycles, showing the precipitate structure. -----	90
30. SEM photomicrograph of VEX0219-3 (Al-19Mg) exposed to ten thermal cycles, showing the overall microstructure.--	91
31. SEM photomicrograph of VEX0219-3 (Al-19Mg) exposed to ten thermal cycles, showing the precipitate structure.--	92
32. SEM photomicrograph of VEX0219-3 (Al-19Mg) exposed to 15 thermal cycles, showing the overall microstructure.--	93
33. SEM photomicrograph of VEX0219-3 (Al-19Mg) exposed to 15 thermal cycles, showing the precipitate structure.---	94
34. SEM photomicrograph of VEX0219-3 (Al-19Mg) showing the results of exposure to six thermal cycles with deformation imposed during the cooling half cycles.-----	95
35. SEM photomicrograph of VEX0219-3 (Al-19Mg) showing the result of thermal cycling concurrent with deformation. -----	96
36. SEM photomicrograph of VEX0219-3 (Al-19Mg) deformed during thermal cycling. -----	97
37. Graphical illustration of the volume fraction of $\beta$ phase present in equilibrium microstructures for compositions of 15 and 19 weight percentage Mg in Al. -----	98



## I. INTRODUCTION

Modern technology constantly calls for stronger yet lighter material for general structural and component applications. The field of materials science is thus constantly seeking to provide new materials which represent improvements in strength-to-weight ratio for industrial applications. The field of aluminum metallurgy and aluminum alloy design has contributed to this search for light materials of moderate strength. Among many alloy systems, the aluminum-magnesium binary system represents a prime candidate for research in this area. The aluminum-magnesium system is unique among the currently important aluminum alloy systems as the primary alloy addition leads to an alloy less dense than the base metal. Thus, as the amount of magnesium present in the alloy is increased, the overall density of the alloy decreases. This is directly opposed to other aluminum alloy systems which increase in overall density as the major alloying addition is increased. Through the concept of dispersion hardening, it is also possible to conceive of increasing strength in alloys using increasing amounts of magnesium.

Because of these properties, the Naval Postgraduate School has initiated on-going research into the properties of the aluminum-magnesium alloy system. The ultimate goal of this research is the development of an alloy demonstrating ambient temperature strength equaling or exceeding currently available



aluminum based alloys, with comparable ductility and lower density. It is further believed that the magnesium content of this kind of alloy can be adjusted to produce a material exhibiting superplasticity at elevated temperatures. Superplasticity refers to the capability to achieve extensive uniform tensile elongation. Tensile elongations of 200% to 2000% have been achieved in other superplastic alloys. This would lead to an alloy possessing excellent ambient temperature characteristics which would be super-formable at elevated temperatures.





## II. BACKGROUND

### A. THE ALUMINUM-MAGNESIUM SYSTEM

The equilibrium phase diagram for the aluminum-magnesium system is shown in Figure 1 for compositions up to 36% magnesium by weight. This portion of the diagram consists of a eutectic reaction, a region of solid solutions of magnesium in aluminum at the left and the intermetallic  $\beta$  phase at the right. The eutectic reaction occurs at a composition of Al-35.0Mg (This designation refers to aluminum plus 35% magnesium by weight, and this method of designating alloy composition will be used hereafter.) and a temperature of 451°C. However, upon reducing temperature only about 30°C to 420°C, a eutectic composition passes into the purely intermetallic  $\beta$  phase. Thus, the system can be viewed as a two-phase mixture of the aluminum solid solution and intermetallic  $\beta$  phases, there being no eutectic constituent.

The most striking feature of this system is the large change occurring in solid solubility of magnesium in aluminum. This solubility reaches a maximum of 14.9% magnesium at the eutectic temperature of 451°C but decreases to 0.82% magnesium at 100°C. During a decrease in temperature of this magnitude, the excess magnesium contained in the aluminum matrix can be expected to precipitate in the form of  $\beta$  phase particles. It is through this mechanism that control of the size and amount of second phase  $\beta$  could be expected to be accomplished.



The aluminum-magnesium solid solution matrix retains the face centered cubic (fcc) structure of the base metal, aluminum. This leads to a ductile but fairly weak matrix upon which to build.

The intermetallic  $\beta$  phase of this system approaches the stoichiometric ratio  $\text{Al}_3\text{Mg}_2$ . There is some disagreement over the crystal structure of this phase. It is considered complex face centered cubic by Willey [1] and further detailed as complex fcc with 1173 atoms per unit cell and a lattice parameter of  $a=28.13\text{\AA}$  by Hansen and Anderko [2]. However, Savitsky [3] states the  $\beta$  structure is hexagonal with 104 atoms per unit cell with  $a=11.32\text{\AA}$  and  $c/a=1.57$ . Both sets of parameters yield a mass density of  $2.27\text{ g/cm}^3$  for the  $\beta$  phase.

Savitsky [3] examined the properties of the  $\beta$  phase through the temperature range of  $20^\circ\text{C}$  to  $430^\circ\text{C}$  and showed the hardness of the  $\beta$  phase decreased rapidly with increasing temperature. Thus, the  $\beta$  phase is a hard, brittle constituent at room temperature; but upon heating to just below the eutectic temperature, it becomes much softer. Data presented by Savitsky [3] shows the  $\beta$  phase having a hardness of four to ten times that of the aluminum-magnesium solid solution at room temperature. Upon heating above  $400^\circ\text{C}$ , this hardness difference is reduced to a factor of two or less, depending on the magnesium content of the solid solution phase. This softening of the  $\beta$  phase is important when attempting to work mechanically alloys containing large volume fractions of



continuous  $\beta$  . That is, these large  $\beta$  regions make the material brittle and unworkable at room temperature. Cracks form and propagate easily in the  $\beta$  regions, leading to fracture during working. At elevated temperatures, in the vicinity of 430°C, softening of the  $\beta$  phase occurs to a level comparable to that of the solid solution matrix. This should allow the  $\beta$  phase to deform in as ductile a manner as the solid solution matrix, eliminating the problem of preferential crack nucleation and growth within the  $\beta$  phase and allowing the material to be extensively hot worked. This results in the possibility of breaking-up and refining the coarse two-phase structure through hot working. The end result should be an alloy demonstrating high strength due to the dislocation barriers presented by the hard, strong  $\beta$  particles but containing some measure of ductility due to the soft, ductile matrix. In addition, the resulting fine, two-phase structure, with both phases demonstrating comparable softness at high temperature, should lead to an alloy demonstrating superplastic or near superplastic qualities when deformed at temperatures above half the absolute melting temperature using low strain rates. This prediction is based on the requirements for superplasticity given, for example, by Brick, Pense and Gordon [4].

Alloys containing greater than 15% magnesium will solidify in a two-phase structure. This can be seen by a vertical line drawn through the phase diagram. For an alloy cast from a melt



containing greater than 15% magnesium, the first solidification will occur in areas having a very low magnesium content. If temperature is decreased slowly enough to allow diffusion to occur in the liquid and also in the solidified regions of the casting, the solid regions will increase in size, and in magnesium content, until the eutectic temperature is reached. Just before reaching the eutectic temperature, the casting will show regions of solidified metal containing almost 15% magnesium in solid solution with aluminum. These regions will be surrounded by liquid containing 35% magnesium. As the eutectic temperature ( $451^{\circ}\text{C}$ ) is crossed, this remaining liquid solidifies. These newly solidified regions will consist of a very small amount of the solid solution phase and about 98%  $\beta$  phase ( $\text{Al}_3\text{Mg}_2$ ). As the temperature continues to decrease, these final regions to solidify will become entirely the  $\beta$  phase.

The previous description of solidification in these alloys assumes that equilibrium is maintained in the casting. This in general requires extremely slow cooling rates. In actual practice, these alloys will solidify in a non-equilibrium manner. A good discussion of the events occurring during non-equilibrium cooling is contained in Brick, Pense and Gordon [4]. The net result of this non-equilibrium cooling is the formation of more of the  $\beta$  phase and less of the solid solution phase. This results in an as-cast microstructure exhibiting large regions of the  $\beta$  phase interspersed with the solid solution phase. Also, the solid solution phase will have a lower concentration of





magnesium than that predicted by the phase diagram. Indeed, it is possible to have  $\beta$  appear, due to the eutectic reaction, in alloys containing substantially less than 15% magnesium under conditions of non-equilibrium cooling.

## B. PREVIOUS RESEARCH

The work of Ness [5], using alloy compositions in the two-phase region from about 15% to 35% magnesium, concluded with very interesting as well as encouraging results. Ness was able to produce a fine, homogeneous dispersion of small, sub-micron sized  $\beta$  particles in the aluminum solid solution matrix through thermomechanical working of material nominally Al-18Mg. This material demonstrated ultimate compressive strengths in excess of 90,000 psi at compressive strains of 40%.

Ness was successful in creating the finely dispersed microstructure shown in Figure 2 by a process of warm rolling. His processing scheme was to heat the material to 425°C and make four passes through a rolling mill set for a reduction of about 1%, turning the material 90° on each pass to maintain a square cross section in the sample. The material would then be reheated to 425°C and the process repeated. Since the rollers could not be heated, the effect of this process was to work mechanically the material as the temperature decreased from 425°C. Also, using this procedure, about 30 repetitions of the basic cycle of heating and rolling were necessary to reach a true strain of 0.94 in the material, which is the value quoted in Ness' thesis.



Figure 2 shows the typical microstructure achieved by Ness using this thermomechanical processing scheme. A fine dispersion of  $\beta$  phase particles has been formed in the aluminum matrix; however, the dispersion is not homogeneous.

Figure 3 shows a more homogeneous dispersion of  $\beta$  resulting from isothermal compression testing at 425°C to a compressive strain of 0.4. This microstructure is excellent and would be expected to produce the desired qualities of this type of alloy.

The thermomechanical history of this material was quite complex. The material had been subjected to about 30 cycles of heating to 425°C, followed by cooling to some lower temperature with concurrent light reductions in rolling being applied during the cooling portion of the cycle until a true strain of about 1.0 was reached. Personal discussions with Ness about his procedure revealed that the material was allowed to equilibrate at 425°C for time periods in excess of 30 minutes. The final homogeneity of the structure was achieved through isothermal deformation at 425°C to a true strain of about 0.4. Thus the total deformation experienced by the material was on the order of a true strain of 1.5.

The net effect of this complex treatment was to eliminate the coarse inter-dendritic  $\beta$  constituents and replace them with a homogeneous distribution of fine, spherodized  $\beta$  particles within the aluminum solid solution matrix. It was originally felt that Ness' procedure was best characterized as one of



breaking-up the coarse  $\beta$  phase regions into submicron sized particles and then redistributing these particles throughout the matrix. It was later shown, however, that Ness' process was actually one involving working of the material as precipitation occurred.

Concurrent with the research discussed in this thesis, Glover [6] investigated the mechanical properties of these alloys after being upset forged to a true strain of 1.5 at a constant temperature of 410°C. Glover's results, as well as some of Ness' work, indicate that the tendency of these materials to become superplastic at elevated temperatures increases as the magnesium content of the alloy increases. However, the 15% and 19% magnesium alloys tested by Glover were extremely brittle at room temperature. Investigations of the cause of this brittleness and methods to improve ambient temperature ductility through thermomechanical processing of these alloys will be discussed in this thesis.



### III. GENERAL DISCUSSION OF RESEARCH

Although this research is best discussed in several parts, there are aspects of this investigation which were common to all parts.

#### A. OBJECTIVES AND PLAN OF INVESTIGATION

As a result of Ness' work, the potential for designing a useful alloy containing greater than 15% magnesium has been demonstrated. However, the procedure used by Ness to work the material resulted in a very complex thermomechanical history and had not been fully characterized by the end of his work. It was necessary to understand which underlying mechanisms were responsible for the creation of the fine, homogeneous dispersion of  $\beta$  phase particles within the primary matrix phase. Such understanding is paramount in further work to optimize the engineering usefulness of this material. The objective of this research project was to isolate the variables in Ness' procedure and study the effects of each one on microstructure. Once the individual effects had been determined, the combined effects could be optimized.

To meet this objective, this research was conducted in four sections:

1. General Isothermal Working Effects
2. Effects of Isothermal Forging Variables
3. Alloy Chemistry Effects
4. Effects of Non-Isothermal Working.





Each of these sections will be discussed separately followed by the overall results and implications of this research.

## B. MICROSCOPY PROCEDURES

The procedures used for microstructural examination were common to the separate sections of this research. Analysis of the microstructure of a sample required, in general, four steps.

### 1. Mounting and polishing

Mounting of samples was accomplished by warm pressing the sample into a right circular cylinder of bakelite, resulting in the sample being centered at one face of a one-inch diameter mount of varying height. This allowed the sample to be held for grinding and polishing.

Grinding was accomplished using emery papers of varying grit sizes in four steps, starting at 80 grit and finishing on 000 grit. Polishing was then conducted by hand, using rotating polishing wheels covered by cloths treated with slurries of alumina and distilled water. The final polishing slurry contained alumina grit of 0.05 micron size. One problem encountered during polishing was pitting of the sample by interaction with the brass polishing wheel. This problem was largely eliminated using a suggestion of Samuels [7] which involved placing a plastic sheet as an insulator between the wheel and the cloth. Using this procedure it was possible to produce a satisfactory finish on



the sample which contained only scratches resulting from the 0.05 micron grit.

## 2. Etching

Several etchants were used during the course of this work. Two etchants, 0.5% HF in 99.5% H<sub>2</sub>O and 10% H<sub>3</sub>PO<sub>4</sub> in 90% H<sub>2</sub>O, when used as recommended in reference 1, gave similar satisfactory results. No chemical etchant was found which would reveal the grain boundaries in the solid solution. The H<sub>3</sub>PO<sub>4</sub> etchant was found to be much better when viewing samples with the scanning electron microscope and is equally satisfactory using a light microscope. Thus in later work, this etchant was used exclusively. The HF etchant appears to be much more prone to the effects of polishing artifacts whereas the H<sub>3</sub>PO<sub>4</sub> etchant removes more of the metal surface, thus eliminating the effects of deformation layers remaining after polishing. Although the H<sub>3</sub>PO<sub>4</sub> etchant required heating to 50°C prior to use, it required less care in polishing and thus represented an overall savings in time. The action of both etchants was to etch away the  $\beta$  regions, the aluminum solid solution being less affected.

## 3. Observation Techniques

Both light microscopic and scanning electron microscopic observation techniques were used in this work. The Bausch and Lomb Balplan incident light microscope with differential interference contrast illumination was used and proved very satisfactory for viewing specimens at magnifications



up to 400 diameters. The ability of this microscope to provide differential interference contrast illumination was a benefit in viewing these samples which, when etched, showed topographical differences between the  $\beta$  and solid solution phases.

The Kent-Cambridge S4-10 Stereoscan scanning electron microscope proved to be the most versatile observation device for analysis of these microstructures. For samples etched with the  $H_3PO_4$  solution, observation was possible at magnifications from 50 to greater than 20,000 diameters with good resolution. Samples etched with the HF solution did not result in sharp enough topographical contrast to be resolved below about 5,000 diameters. It was found that an electron accelerating voltage of 6.5 KV gave best results and eliminated most of the effects caused by the differences in electrical conductivity between the aluminum rich regions and magnesium rich regions.

Both the light and electron microscopes were fitted with camera adaptors which accepted Polaroid type 55 (ASA50) film. All record micrographs were made using this film.

### C. SOURCE OF MATERIALS

Materials used in this investigation were derived from two sources. Some attempts at casting billets of desired nominal compositions were made in the Materials Science Laboratory at the Naval Postgraduate School using procedures developed by Ness [5]. The most successful of these was a one-inch square billet, four and one-half inches in length, designated BG-18A.



This billet was cast using 155.4 grams of 99.99% pure aluminum and 34.1 grams of commercially pure magnesium to give a resulting nominal composition of Al-18Mg. Due to an inability to cast larger sized billets, arrangements were made with Kaiser Aluminum and Chemical Corporation's Center for Technology to provide two castings of nominally 15% and 19% magnesium alloys. These alloys were cast in 2-1/4 x 4-1/2 x 12-7/8 inch graphite book molds. To reduce magnesium oxidation, the melts for these alloys were treated with 0.0005% berillium by weight. The resulting alloys were designated VEX0219-2(Al-15Mg) and VEX0219-3(Al-19Mg). One other casting of Al-11Mg was procured, but the volume fraction of the  $\beta$  phase present at this composition was too low to be considered in this work. A discussion of this alloy and its mechanical properties may be found in work done by Glover [6].

The major difference between these castings and billets cast at NPS was the ability to create a finer microstructure in the smaller billets. This is due to the more severe chill resulting from the smaller billet size.





#### IV. ISOTHERMAL WORKING

##### A. DISCUSSION

Isothermal deformation or hot working is a common means of producing a fine, two-phase structure in eutectic alloy systems. Alden [8] discusses several eutectic systems and the ability to produce fine two-phase structures in these materials through hot rolling or hot extrusion processes. Cipriani [9] demonstrated the feasibility of producing a fine two phase microstructure in an Al-17.5Cu alloy by warm rolling. In all of these examples the cast structure contained a fine eutectic constituent dispersed in one of the terminal phases of the binary system. This is in contrast to the Al-Mg system in which the eutectic is in reality not a mixture of two phases but wholly made up of an intermetallic phase.

Previous work in the Al-Mg alloy system had not revealed the specific mechanism of microstructural refinement which had led to production of a fine, homogeneous dispersion of  $\beta$  particles. It was theorized, based on documented results with other eutectic systems, that the break-up of the coarse  $\beta$  structure and the production of the fine, homogeneous structure were both a result of the same mechanism. That is, during deformation stresses were transmitted to the  $\beta$  regions through the matrix. The  $\beta$ , relatively ductile at warm working temperatures, would break-up into small particles. By continued application of



stress, these particles would then be redistributed throughout the matrix in a homogeneous dispersion. Temperature becomes an important part of this process. As temperature increases, the matrix material should increase in ductility and show less tendency for crack propagation. But the concepts of recrystallization and growth imply that the temperature be kept as low as possible to result in the finest grain structure in the matrix itself. Thus, there should be some optimum temperature at which the mechanism of breaking-up and distributing of the  $\beta$  structure would be operable while the aluminum matrix would still be ductile enough to prevent any cracks in the  $\beta$  regions from propagating through the material, leading to failure during working. This optimum temperature would also be low enough in the recrystallization region that working of the aluminum matrix would result in a fine grained matrix structure. If this theory were to be proven feasible by experiment, it would mean that alloys of aluminum with magnesium contents varying from 15% to 30% by weight could be successfully hot worked to create a fine dispersion of the  $\beta$  phase within the aluminum solid solution. Research could then be directed toward the optimization of mechanical properties of alloys within this range of compositions.

Two factors were evident from the work of Ness. The process he used involved deformations of the order of 1.5 true strain, and the material he rolled was heated to a temperature



of 425°C. These two factors were considered when the experimental investigation was designed to verify the stated theory.

#### B. EXPERIMENTAL PROCEDURE

Since the effects of varying temperature were to be eliminated as much as possible in this study of isothermal working effects, the rolling procedure of Ness could not be used. This was a limitation imposed by the only available rolling mill which did not have the capability to heat and maintain the rollers to a given working temperature.

To accomplish the objective of temperature control during deformation, a hot upset forging apparatus was developed. This apparatus is shown in Figure 4. This arrangement consisted of two steel platens installed on a Baldwin-Tate-Emery universal testing machine having a 60,000 pound load capacity in compression. Two resistive heating elements were embedded in grooves cut in the back of each platen.

Forging billets were cut from castings and then milled to a parallelepiped shape, 2 inches in length and 3/4 inch on each side. Billets of this size could be placed upright between the forging platens and upset forged to a flat, pancake shape with a thickness corresponding to a true strain of 1.5 without exceeding the load limit of the machine.

After upsetting, forgings were hot rolled by first heating to a rolling temperature of either 300°C or 425°C. Only one pass was made through the mill at each



roller setting, and the material was reheated to the rolling temperature between each pass. Using this procedure, the hot material was in contact with the cold steel of the rolling mill for a maximum of ten seconds prior to deformation. Conditions of isothermal deformation were thus approximated by rolling in this manner. It was the objective of the rolling procedure to produce material having been subjected to total deformations in isothermal working of up to 3.0 true strain. However, rolling was unsuccessful due to severe cracking of the material after only a few passes. This failure was attributed to the severe thermal stresses created by contact with the cold rollers.

#### C. RESULTS OF ISOTHERMAL WORKING

The most significant result of attempting to produce a desirable microstructure by isothermal working was a failure to eliminate the coarse  $\beta$  regions existing in the material as cast. Figure 5 illustrates the microstructure of the cast billet BG-18A which was nominally Al-18Mg. This photomicrograph was typical of cast structures in these alloys, although this billet was smaller than those received from Kaiser, and this resulted in a more severe chill and somewhat finer as-cast microstructure. Figure 6 illustrates the microstructure of this alloy resulting from a 20 hour soaking treatment at 400°C followed by upset forging at 400°C to a true strain of 2.0. The coarse  $\beta$  regions have not been eliminated; in fact, comparison with the cast





structure indicates some coarsening of the  $\beta$  regions. Some formation of  $\beta$  within the aluminum matrix is evident, although this appears to have taken the form of precipitation at the grain boundaries. Figure 7 shows the microstructure after forging at 400°C, followed by a hot rolling reduction of 10% at 300°C. Again, no progress is evident in elimination of the coarse  $\beta$  regions; however, much more  $\beta$  has been formed in the aluminum matrix. This difference between working at 400°C and 300°C can be explained by the decrease in solid solubility of magnesium in aluminum occurring between these two temperatures, leading to more  $\beta$  precipitation at the lower temperature.

The results of the isothermal deformation experiments conducted to this point were disappointing. The upset forging procedure was successful in that the material did not outwardly exhibit any signs of failing during working. However, all attempts at rolling between 300°C and 425°C resulted in excessive cracking of the material and eventual total failure by the breaking-up of the material. Figure 8 is an example of material which failed during rolling. Also, microstructural refinement of the coarse  $\beta$  was not achieved by any means. It was still believed that there might exist some combination of isothermal working conditions which would result in the desired microstructural refinement.



## V. THE EFFECT OF HOT FORGING ON MICROSTRUCTURE

### A. DISCUSSION

Experiments to this point had indicated little or no improvement in microstructure as a result of isothermal working. However, these experiments were not deemed conclusive proof that the coarse  $\beta$  in the cast structure could not be broken-up and refined by this method. It was decided that a controlled set of experiments would be required to prove conclusively whether or not isothermal working was a valid means of microstructural refinement in this particular alloy system.

Four variables were chosen for investigation as follows: total strain, strain rate, temperature and alloy composition. It was also felt that it might be possible following this experiment to relate the degree of microstructural refinement observed to expected strength levels of the alloy. Dieter [10] illustrates the dependence of strength on strain rate and temperature through the Zener-Hollomon parameter  $Z$ .  $Z$  is given by

$$Z = \dot{\epsilon} \exp (\Delta H/RT) \quad (1)$$

where  $\dot{\epsilon}$  is the true strain rate,  $\Delta H$  is related to the activation energy required for plastic flow,  $R$  is the universal gas constant and  $T$  is the absolute temperature.



## B. EXPERIMENTAL PROCEDURES

The two cast billets received from Kaiser, VEX0219-2 (Al-15Mg) and VEX0219-3 (Al-19Mg), were used as the source of material for these experiments. Twenty-seven parallelepiped shaped compression specimens 0.3 inches long and 0.2 inches on each side were milled from each cast billet.

To allow control of the variables strain, strain rate and temperature, an Instron Model TT-D floor model testing machine was used. This Instron is a constant crosshead speed testing machine modified for hot compression testing under isothermal conditions by the addition of a Marshall split furnace capable of temperatures up to 650°C. An integral synchronous chart recorder provided continuous curves of load versus time which could easily be converted to compressive stress-strain curves. Control of furnace temperature was provided by a Model 49 Omega proportioning control unit. This arrangement is shown in Figure 9. The specimen chamber, shown in Figure 10, contained two tungsten carbide platens which contacted the specimen during compression. To help reduce the effects of triaxiality during deformation, Molly Dry Film Lubricant, a commercial product, was used between the platens and the specimen surfaces.

Temperatures were chosen for investigation based on a ratio similar to homologous temperature which is the ratio of absolute temperature to absolute melting temperature. Instead of absolute melting temperature, absolute eutectic temperature



(724°K) was used. This ratio could then be viewed as a fraction of the absolute eutectic temperature. Using this ratio, values of 0.65 (200°C), 0.75 (270°C) and 0.95 (415°C) were chosen to represent temperatures throughout the recrystallization range of the material. The lower two temperatures were chosen to find a region where recrystallization would occur but growth would be slow. The highest temperature was chosen due to the success of Ness' working initially at 425°C.

Strain values of 0.5, 1.0 and 1.5 were chosen for study. These strains represented a sampling of those attainable on the testing machine with the initial test specimen geometry. Constant true strain rate could not actually be achieved since the Instron is a constant crosshead speed machine, and true strain rate would thus increase as the sample was deformed. It was possible to determine the average strain rate at the completion of each test. Head speeds of 0.2, 0.05 and 0.01 inches per minute were chosen which resulted in average strain rates of  $2 \times 10^{-2} \text{ sec}^{-1}$ ,  $5 \times 10^{-3} \text{ sec}^{-1}$  and  $1 \times 10^{-3} \text{ sec}^{-1}$ , respectively. Test sample designations and testing conditions are given in Table I.

After testing, each sample was examined using the microscopy procedures detailed previously. Quantitative microscopy was used on several samples of the VEX0219-3 alloy to see if a phenomenological relationship could be developed between the microstructural features resulting from the test and the Zener-Hollomon parameter  $Z$ . As a measure of microstructural





Table I - Test Conditions for Examination of the  
Effect of Strain, Strain Rate and Temperature on Mi-  
crostructural Refinement

VEX0219-2 Sample No.	VEX0219-3 Sample No.	TEMPERATURE °C	HEAD SPEED In/Min	TOTAL STRAIN In/In
31	61	200	0.2	0.5
32	62	200	0.2	1.0
33	63	200	0.2	1.5
34	64	200	0.05	0.5
35	65	200	0.05	1.0
36	66	200	0.05	1.5
37	67	200	0.01	0.5
38	68	200	0.01	1.0
39	69	200	0.01	1.5
40	70	270	0.2	0.5
41	71	270	0.2	1.0
42	72	270	0.2	1.5
43	73	270	0.05	0.5
44	74	270	0.05	1.0
45	75	270	0.05	1.5
46	76	270	0.01	0.5
47	77	270	0.01	1.0
48	78	270	0.01	1.5
49	79	415	0.2	0.5
50	80	415	0.2	1.0
51	81	415	0.2	1.5
52	82	415	0.05	0.5
53	83	415	0.05	1.0
54	84	415	0.05	1.5
55	85	415	0.01	0.5
56	86	415	0.01	1.0
57	87	415	0.01	1.5



refinement, the mean free path,  $\lambda$ , between precipitate particles produced in the aluminum solid solution matrix was chosen as a test parameter. Photomicrographs were taken at an appropriate magnification to exclude any coarse  $\beta$  particles remaining from the cast structure from the field of view. Calculation of the parameter  $\lambda$  was accomplished from a combination of point counting and lineal analysis observations. Following the development of Guy & Hren [11], the following equation was developed for calculating the mean free path,  $\lambda$ , between discrete, homogeneous, non-touching, particles in the matrix:

$$\lambda = \frac{1 - P_p}{N_1} \quad (2)$$

All parameters in this equation refer to values for the  $\beta$  phase.  $P_p$  is the number of intersections of the  $\beta$  particles with a random point grid divided by the total number of points in the grid.  $N_1$  is the number of  $\beta$  particles intersecting a random test line per unit length of test line.

### C. RESULTS OF HOT FORGING

Figures 11 and 12 show representative microstructures of the VEX0219-2 and VEX0219-3 castings. As was expected, the alloy containing 19% magnesium exhibited much more of the  $\beta$  phase than was present in the alloy containing 15% magnesium.



## 1. Temperature Effects

Figure 13 illustrates the microstructural changes observed in VEX0219-2 (Al-15Mg) due to change in testing temperature. All samples had experienced deformation at the same rate and to the same total strain. The lower temperature deformation resulted in more refinement of the coarse  $\beta$  regions, although the  $\beta$  remained in the form of colonies of finer particles and was not redistributed throughout the matrix. The high temperature deformation resulted in no effective breaking-up of the  $\beta$  structure.

Figure 14 illustrates the comparative flow stress levels resulting from the three test temperatures. Considerable softening occurred in the material as the temperature was increased. These flow stress curves were not corrected for the triaxiality effects of barrelling of the compression samples, which explains the sharp upward curvature beyond strain values of about 0.75.

Figure 15 illustrates the effect of temperature on the VEX0219-3 (Al-19Mg) alloy. Again, constant strain and deformation rate were imposed with only temperature being variable. The effect of temperature variation on this alloy was similar to that shown for the VEX0219-2 (Al-15Mg) alloy. The major difference was the increased amount of  $\beta$  phase present in this alloy resulting in a more homogeneous appearing microstructure. Coarse  $\beta$  regions were broken-up but remained in large enough, continuous structures to result in brittle behavior of the alloy. In contrast to the 15% alloy, this alloy demonstrated more



breaking-up of the continuous  $\beta$  regions at the highest temperature, resulting in a more discrete, equiaxed  $\beta$  structure.

Figure 16 again illustrates the extreme amount of softening which occurred as temperature was increased.

## 2. Strain Effects

Figure 17 illustrates the effect of increased total strain on the VEX0219-3 (Al-19Mg) alloy samples tested to various strains at constant temperature and deformation rate. The sample deformed to a strain of 0.5 resulted in no apparent change from the cast microstructure. As strain was increased to 1.0, the coarse  $\beta$  regions were just starting to break-up, and fracture lines were observed in the  $\beta$  regions. By a strain of 1.5, this fracturing and breaking-up of the  $\beta$  regions had resulted in considerable refinement of the  $\beta$  structure.

## 3. Strain Rate Effects

Figure 18 illustrates the observed microstructures resulting in samples which were tested at constant temperature and to the same total strain. More breaking-up and spreading of the coarse  $\beta$  regions have occurred in the sample tested at the slower head speed; however, the strain rates used did not seem to have a significant effect on refining and homogenizing the microstructure. More extreme variations in strain rate may have resulted in a better characterization of the effects of strain rate on microstructural refinement.

Figure 19 illustrates the variation in flow stress resulting from the head speeds used in testing. This variation





is typical of the strain rate sensitivity exhibited by these materials at elevated temperatures. A complete analysis of the mechanical properties, including strain rate sensitivity, was conducted by Glover [6].

#### 4. Precipitation Structures

The quantitative analysis of  $\beta$  phase precipitation within the aluminum solid solution matrix was conducted using all of the samples of VEX0219-3 (Al-19Mg) which were tested to a strain of 1.5. As previously explained, the mean free path,  $\lambda$ , was calculated, and the resulting values are given in Table II. An attempt was made to correlate this data with the Zener-Hollomon parameter,  $Z$ , but no phenomenological relationship could be found. Figures 20 through 22 illustrate the types of precipitate structures which resulted from this testing. Sample number 69 (Figure 20c) resulted in the finest precipitate structure. A very coarse precipitate structure resulted at high temperature as illustrated by Figure 22.

#### D. DISCUSSION OF TEST RESULTS

The observations of the microstructures which resulted from isothermal compression of the test samples showed that the trends of microstructural refinement were similar for both alloy compositions. The most significant trend observed was due to the variation of temperature. In both refinement of coarse  $\beta$  regions and creation of a fine  $\beta$  structure within the aluminum solid solution, the lower temperatures proved more



TABLE II - Mean Free Path Data for the  
19% Magnesium Alloy as  
a Function of Temperature and Strain Rate

TEST SAMPLE NUMBER	TEST TEMPERATURE °C	STRAIN RATE SEC <sup>-1</sup>	$\bar{\lambda}$ μm
63	200	$2 \times 10^{-2}$	17.46
66	200	$5 \times 10^{-3}$	3.40
69	200	$1 \times 10^{-3}$	0.90
72	270	$2 \times 10^{-2}$	2.02
75	270	$5 \times 10^{-3}$	2.01
78	270	$1 \times 10^{-3}$	2.18
81	415	$2 \times 10^{-2}$	9.96
84	415	$5 \times 10^{-3}$	16.00
87	415	$1 \times 10^{-2}$	17.71



effective. Precipitation of the  $\beta$  phase from the aluminum solid solution can be predicted from the equilibrium phase diagram. Due to the change in solid solubility of magnesium in aluminum with temperature, it would be expected that the amount of  $\beta$  which forms in the solid solution matrix is a function of the temperature to which the material is reheated after casting. From this, it would be expected that more precipitation would occur at lower forging temperatures. However, the results of this experiment indicated that deformation conditions also had an effect on the structure of the  $\beta$  phase created within the solid solution matrix. This observation was made when samples tested at the same temperature exhibited great variations in microstructure. This indicated that the mechanisms involved were not solely temperature activated.

The most significant result of this experiment was the inability to eliminate the coarse  $\beta$  phase from the microstructure. Based on this observation, it was shown that the mechanism of microstructural refinement was not simply a matter of break-up and redistribution of the  $\beta$  phase resulting from the cast structure. Analysis of the flow stress exhibited during testing indicated a possible explanation for the varying observations of how the  $\beta$  phase structure had been broken-up. Little or no fracturing of  $\beta$  regions was observed at the highest test temperature. As the test temperature was decreased, however, a greater tendency toward break-up and separation of the  $\beta$  phase into smaller, discrete particles was shown. This can be



explained by a study of the flow stress behavior of the material in the cast state. The process of breaking-up of the microstructure requires a transmission of force from the deformation machinery to the regions of coarse  $\beta$  phase. The amount of softening which was observed as temperature was increased implied that the matrix material may have become too weak and ductile at the higher temperature to transmit sufficient force to the  $\beta$  regions. Thus, at the lower temperatures, where the matrix was stronger, a tendency toward more breaking-up of the  $\beta$  phase was observed.





## VI. THE EFFECT OF ALLOY CHEMISTRY

Discussions with Ness indicated that the castings which had been used in his experiments were made from a combination of 1100 aluminum alloy and magnesium of commercial purity. This led to the conclusion that the success of Ness, and the apparent failure to reproduce it in these experiments, may have been due in part to differences in alloy chemistry. It was decided therefore to make a study of the effects of alloy chemistry on the microstructure of these alloys.

### A. CHEMICAL ANALYSIS

#### 1. Sample Selection

Samples were chosen for analysis from two of Ness' castings, the BG-18A casting made as a part of this research and the three castings received from Kaiser. Based on the weighed proportions used to make the melts prior to casting of the billets, the nominal compositions were determined to be as follows: Ness #7, Al-20Mg; Ness #8, Al-20Mg; BG-18A, Al-18Mg; VEX0219-1, Al-11Mg; VEX0219-2, Al-15Mg; VEX0219-3, Al 19Mg.

#### 2. Analysis Methods

Two methods of analysis were eventually used, atomic absorption and emission spectroscopy.

##### a. Atomic Absorption

Atomic absorption analysis was conducted using the Perkin-Elmer Atomic Absorption Spectrophotometer, model PE-303,



available at the Naval Postgraduate School. This method was also used in part of an analysis conducted by the Naval Weapons Support Center, Crane, Indiana [12]. Analysis by atomic absorption (AA) methods required that a weighed amount of the sample be dissolved in a small amount of hydrochloric acid (HCl) and this solution diluted with deionized distilled water. Dilutions of the six samples for analysis at the Naval Postgraduate School were prepared by obtaining turnings of the sample castings. A sample of these turnings was collected having a total weight of between 0.5 and 1.0 grams. The exact weight of these samples was determined to within 0.00005 grams. The weighed metal samples were dissolved in about 20 ml of concentrated HCl solution. After the metal had dissolved, the solution was diluted to a total volume of 500 ml. Finally, the solution was stirred vigorously for 15 minutes to eliminate any stratification. The resulting solutions had concentrations of unknown metal ions ranging from 1000 to 2000 ppm.

The unknown solutions were analyzed for concentrations of Mg, Fe and Cu ions by comparison with commercial standards. This comparison process involved atomizing a small portion of the unknown solution in a nitrous oxide ( $N_2O$ ) flame. Light from a cathode made of the same material as that being tested for was passed through the flame, and a detector recorded the amount of absorption which occurred. This procedure was repeated for dilutions made from a standard solution of known



concentration resulting in a standard calibration line from which the concentration of the element in the unknown solution was calculated. For each element analyzed, several hand dilutions of the unknown as well as standard solutions were necessary to bring the concentration levels into the range of known linear behavior under absorption conditions. This requirement was the major source of errors in this analysis method.

#### b. Emission Spectroscopy

The Naval Weapons Support Center [12] analyzed the six castings for Mg and Fe using AA methods and for Zn, Si, Cu, Cr, Mn, Ti and Ni using emission spectroscopy. This later method involved striking a spark between an electrode and the solid sample surface. The spectrum of light given off by this spark was then compared to spectra of known samples and quantitative measurements of concentration made by comparison of spectral line intensities.

### 3. Results of Chemical Analysis

The various results achieved by all means of chemical analysis are presented in Table III. The results for Mg content showed large variations between results obtained at the Naval Postgraduate School and Naval Weapons Support Center. There was also little correlation between the chemical analysis for Mg and the nominal compositions based on amounts of constituents which were used in the melts for these castings.



TABLE III - ALLOY COMPOSITIONS

ALLOY (Nominal Mg)	Mg	Fe	Zn	Cu	Si	Cr	Mn	Ti	Ni
VEX0219-1 (11)	4.68 (6.7)	0.20 (0.06)	0.087	0.053 (0.009)	0.13	0.013	0.020	0.004	0.037
VEX0219-2 (15)	13.02 (16.7)	0.14 (0.14)	0.037	0.140 (0.016)	0.085	0.048	0.045	0.005	0.063
VEX0219-3 (19)	16.25 (20.1)	0.13 (0.13)	0.014	0.020 (0.012)	0.068	0.008	0.022	0.004	0.024
Ness #7 (20)	14.44 (18.0)	0.28 (0.28)	0.170	0.081 (0.016)	0.240	0.008	0.061	0.018	0.022
Ness #8 (20)	13.89 (16.4)	0.28 (0.29)	0.610	0.020 (0.044)	0.100	0.007	0.051	0.017	0.022
BG-18A (18)	(18.0)	(0.07)	No analysis by Naval Weapons Support Center (0.020)						

## Notes:

1. All values are weight percentages.
2. Numbers in parentheses for Mg, Fe, and Cu are the results of AA analysis conducted at the Naval Postgraduate School.
3. Nominal Mg contents are based on weights of melt constituents.





Coutu and Krashes [13] state that AA analysis becomes increasingly inaccurate as the concentration of the unknown element increases above about 0.5%. This is due to the manual dilutions required to bring the concentration level into the linear region of the instrument. The only conclusion drawn from the Mg data was that the material with which Ness was successful may conceivably have been as low as 15% to 16% magnesium vice the melt composition of 20%. The significance of this was not fully demonstrated until later research had been completed.

The results for other elements were deemed to be fairly accurate. The two analyses conducted for Fe, both using AA techniques, showed excellent correlation. The analyses for Cu were done using different methods, and this is likely the origin of the differences appearing in the results.

It was concluded from these results that Ness was working with alloys containing greater amounts of Fe, Zn and Cu than those used for this study. It was decided, therefore, to investigate briefly the effects of these alloy additions.

## B. EFFECTS OF ALLOY CHEMISTRY DURING FORGING

### 1. Casting of Test Alloys

Three alloys were cast using the VEX0219-3 (Al-19Mg) Kaiser alloy as the base. For examination of the effects of Fe additions, an alloy containing 5% Fe was cast using 99.99% pure aluminum and pure iron filings. This master alloy was then cast with the VEX0219-3 alloy to create an alloy having



a nominal composition of Al-17.8Mg-0.3Fe. This casting was accomplished by Glover [6] and is included here for continuity. A second master alloy was cast to a nominal composition of Al-5Zn and used to create an alloy nominally Al-18Mg-0.5Zn. Finally, 2024 aluminum alloy stock and the VEX0219-3 alloy were combined to create an alloy nominally Al-19Mg-0.13Cu.

## 2. Effects of Working on Test Alloys

Each of the test alloys and one billet of the VEX0219-3 alloy were upset forged at 300°C to a strain of about 1.5 and examined microscopically to determine differences in microstructure which resulted from the third alloy additions.

Figure 23 illustrates the microstructure present in the VEX0219-3 alloy before and after upset forging. As noted previously, no significant change in the structure of the coarse  $\beta$  phase regions was evident.

Figure 24 illustrates the microstructure which resulted in the Al-17.8 Mg-0.3Fe alloy. Quite a bit of breaking-up of the  $\beta$  phase regions had taken place; however, the  $\beta$  phase still was too coarse to be useful in creating a non-brittle alloy. The results obtained with the Al-18Mg-0.5Zn and Al-19Mg-0.13Cu alloys (Figures 25 and 26) were similar to those of the alloy with added iron. Each forged alloy resulted in a more broken-up, equiaxed  $\beta$  phase structure than that of the casting. However, in no case was the microstructure even close to the fine structure obtained by Ness. This indicated that the success of



Ness was not entirely a result of alloy chemistry. Insufficient experimentation was conducted, however, to eliminate alloy chemistry as an important variable in this alloy system. It could be concluded at this point that alloy chemistry, as it applied to third alloy additions, was not the sole controlling difference between the success of Ness and the failure in this work to duplicate his microstructure.



## VII. THE EFFECTS OF NON-ISOTHERMAL TREATMENTS

In summarizing the work of Ness on this alloy system, it was noted that the process which led to Ness' eventual success was one of working the material while temperature was changing. It has been demonstrated that working of these materials isothermally does not eliminate the coarse  $\beta$  phase regions resulting in casting. The next section of this investigation was therefore directed toward determining the effects of varying thermal history alone and varying thermal history combined with deformation, on microstructure.

### A. MATERIAL THERMAL RESPONSE CHARACTERISTICS

As a prerequisite to conducting experiments which involved heating and cooling this material, it was necessary to determine more accurately the thermal response of this material when subjected to thermal gradients.

One billet of the VEX0219-2 (Al-15Mg) alloy was prepared as a test billet. The dimensions of this billet were the same as had previously been used for standard upset forging billets (2 inches x 3/4 inch x 3/4 inch). A 1/16 inch diameter hole, 3/8 inch deep, was drilled in the center of one face of this billet. A small Chromel-Alumel thermocouple was inserted into this hole such that it would measure the temperature at the center. To help eliminate the effect of air around the thermocouple, asbestos powder was embedded into the hole around the





wires. This resulted in the thermocouple measuring the temperature of the metal at the center of the billet.

Several experiments were conducted. The first of these was to determine the amount of time required to obtain through-heating at 425°C starting with the billet at room temperature. The results of this experiment are shown by curve A of Figure 27. This experiment demonstrated that at least 30 minutes was required for these alloys to be equilibrated at 425°C. Next, the sample was removed from the furnace at 425°C and placed between the upset forging platens heated to 200°C. It was demonstrated, as shown by curve B of Figure 27, that 16 minutes were necessary for the center of the test billet to reach 200°C. The surface temperature of the billet could be expected to reach the platen temperature much more rapidly. Finally, the test billet was again equilibrated at 425°C, then removed from the furnace and laid on a 1/4 inch steel plate at room temperature. This was done to simulate the conditions to which Ness had subjected the material in rolling. These results are shown by curve C of Figure 27. From this data and a study of the time necessary to complete four passes through the rolling mill, it was possible to estimate the temperature range which Ness' material had experienced during rolling. Since four passes through the rolling mill require about 45 seconds, Ness' material, which was smaller in cross section than the test sample, was evidently worked as the temperature dropped from 425°C to between 200°C and 250°C.



## B. THERMAL TREATMENT EFFECTS

An appreciation of the effects of non-equilibrium cooling on the microstructure of the cast alloys led to the conclusion that some refinement could be achieved in the coarse  $\beta$  phase structure simply by subjecting the material to a process of thermal cycling. The microstructure of the cast alloys was a non-equilibrium structure containing more  $\beta$  phase and less of the aluminum solid solution phase than would be present at equilibrium. By reheating the alloy to a temperature near the eutectic temperature, it was thought that at least some of the magnesium in the coarse  $\beta$  regions would be eliminated by the increase in solid solubility of the aluminum. Subsequent cooling to a temperature of about 200°C would cause some precipitation of the  $\beta$  phase within the solid solution matrix due to the decrease in solid solubility as reflected by the phase diagram. Furthermore, if holding times were short at this lower temperature, insufficient diffusion of the magnesium would take place to allow the  $\beta$  regions to grow appreciably. Finally, through repetition of this process, it was hoped that the coarse  $\beta$  phase regions could be reduced in size. An experiment was conducted to examine the actual effects of this process.

### 1. Experimental Procedures

Three samples of the VEX0219-3 (Al-19Mg) alloy were prepared having dimensions of 3/4 inch x 1/2 inch x 3/8 inch. Two furnaces were set, one at 425°C and the other at 200°C.



These temperatures were chosen to approximate the temperature range assumed for Ness' work.

The three samples were then placed in the 425°C furnace for one hour. At the end of this time, the samples were transferred to the 200°C furnace and again left for one hour. This constituted one cycle. Through repetition of this procedure, samples were produced which had been exposed to five, ten and fifteen cycles through this temperature treatment. As each sample was removed from the last treatment at 200°C, it was allowed to air cool.

## 2. Results of Thermal Treatment

The cast structure for the VEXO219-3 alloy is shown in Figure 23. Figure 28 shows the microstructure which resulted after five cycles of thermal treatment. As expected, some decrease in the size of the coarse  $\beta$  phase regions had occurred. This was evidenced by the regions where the solid solution appears to be growing together. Also, a precipitate structure was forming in the solid solution. Figure 29 is a better view of this precipitate structure. Analysis of this microstructure reveals that the precipitation, due to the change in solid solubility from 425°C to 200°C, appears in two forms. Grain boundary precipitates are visible and appear to be rather equiaxed and coarser than the other form. Long, thin precipitates, typical of Widmannstätten type growth, are also present. These precipitates grow in definite crystallographic orientations and appear to favor two perpendicular crystal planes in the fcc matrix.



In some areas, these plate-like precipitates have become quite dense which results in a very fine microstructure.

Figure 30 illustrates the microstructure resulting from ten thermal cycles. The reduction of the  $\beta$  phase regions has continued, and the precipitate structure has become more homogeneous. Figure 31 illustrates the appearance of this precipitate structure. As the Widmannstätten plates become more dense, they evidently combine to form more equiaxed particles of sub-micron size.

Figure 32 shows the microstructure resulting after 15 temperature cycles. The coarse  $\beta$  regions have again been reduced but, even by this point, not eliminated. The precipitation structure shows signs of coarsening in this stage of processing. Figure 33 shows that the precipitates have begun to coalesce and grow. This stage of precipitate development was believed to be undesirable, and the maximum number of cycles to which this material could be subjected to maximize the reduction of coarse  $\beta$  phase regions and minimize the growth of the precipitate structure was thought to be between ten and fifteen cycles.

### C. THERMOMECHANICAL TREATMENT EFFECTS

In the processing scheme used by Ness, the material was taken from a 425°C furnace and subjected to deformation by cold rollers. This resulted in the material being deformed as temperature decreased. It had been shown to this point that the temperature variations to which the material was subjected







would not in themselves lead to elimination of the coarse  $\beta$  regions existing in the cast structure. If these regions could be eliminated by a combined process of thermal cycling and deformation, it would show that the mechanism which led to Ness' success was actually a combination of thermal effects assisted by deformation. That is, the effects of the change in solid solubility, coupled with the breaking-up of the coarse  $\beta$  regions and deformation assisted precipitation, would lead to a fine homogeneous dispersion of the  $\beta$  phase in the aluminum solid solution. To test this theory, one experiment was conducted to combine the effects of thermal treatment and deformation.

#### 1. Experimental Procedures

In order to allow this experiment to be conducted under relatively controlled conditions, deformation of the material was carried out using the upset forging scheme. As mentioned earlier, Ness' procedure had been characterized as deformation coupled with a temperature decrease in the material from 425°C to about 200°C. In the heat flow experiments, it had been demonstrated that 16 minutes were necessary for the center of a standard upsetting billet to drop from 425°C to 200°C when placed between 200°C forging platens. Also, Ness had taken four passes through the rolling mill during this temperature drop. Using these factors, the procedures for this experiment were developed.

It was decided to use the VEX0219-3 (Al-19Mg) alloy for this test as this would provide comparability with previous results.



A standard upsetting billet, 2 inches x 3/4 inch x 3/4 inch , was placed in a furnace set for 425°C and allowed to equilibrate at this temperature. The billet was then placed between the forging platens which were set to 200°C. During the 16 minutes required for the billet to cool to 200°C, four stages of deformation were applied. Each stage was calculated to be one-fourth of the total deformation required to reach a true strain of 0.25 by the end of the fourth stage. The deformation stages were applied such that the first would occur as the material temperature dropped from 425°C to 350°C, the second from 325°C to 300°C, the third from 275°C to 250°C and the fourth from 225°C to 200°C. During the period between each stage, the platens were stopped, thus allowing the material to recover microstructurally to some degree prior to the next stage.

After each series of deformations the billet was measured with a micrometer and placed in the 425°C furnace for 30 minutes. Then the process was repeated. It was planned to continue this process until a true strain of 1.5 was reached. However, during the third stage of the first series of deformations, cracks began appearing at the edges of the billet. These cracks continued to widen as the process was continued. Also, the load limit of the machine was reached on the sixth series of deformations.



## 2. Thermomechanical Working Results

Figure 34 shows the microstructure which resulted from this thermomechanical processing. The coarse  $\beta$  phase regions have been fractured and have become discontinuous but still remain in the form of networks of five to ten micron sized particles. There is also evidence in this micrograph of the formation of a fine precipitate structure within some areas of the solid solution regions.

Figure 35 shows in more detail the mechanism of breaking-up of the  $\beta$  structure. The  $\beta$  region shown was continuous in the cast structure. After thermomechanical treatment, this region had been fractured and the aluminum solid solution has entered the fissures to provide boundaries within the  $\beta$ .

Figure 36 shows that the precipitate structure which had formed in the aluminum matrix was one of discrete equiaxed particles of about 0.1 micron. Some of these particles had grown together to form particles of up to 1.0 micron in diameter. There is no evidence of the Widmannstätten type of structure observed to result from purely thermal treatment. This indicates that there is a difference in the precipitation, nucleation and growth mechanisms between these two processes. The smaller, more equiaxed particles existing after thermomechanical treatment are more desirable in a final microstructure thus implying that some type of deformation assisted nucleation is the desirable working method in these alloys.



## VIII. SUMMARY AND DISCUSSION OF RESULTS

All of the research conducted for this thesis was done in an attempt to understand better the mechanisms and phenomenology underlying the successful results obtained in earlier research by Ness. The microstructures of these Al-Mg alloys after melting and casting are unsatisfactory. The two-phase microstructure consists of regions of Al-Mg solid solution with coarse, continuous, networks of the brittle intermetallic phase. Ness was able to transform this structure into one exhibiting a fine, homogeneous, dispersion of micron sized second-phase particles in a matrix of the Al-Mg solid solution. This microstructure exhibited no residual coarse second-phase from the cast structure.

Ness' procedure, which produced this type of microstructure, involved a very complex thermomechanical history. The steps taken in this research were intended to isolate the variables of Ness' process to determine the individual effects of each variable on the microstructure of the alloy.

The effects of isothermal working were studied in detail. Temperatures were chosen from a broad range and indicated a trend toward finer microstructure as temperature decreased. The materials were subjected to various strains which covered in detail the range from zero strain to a true strain of 1.5. Some earlier samples were deformed to a strain of almost three. Again the trend appeared to be finer microstructure with





increasing strain. Strain rates were varied over a fairly narrow range, and little microstructural variation resulted. The end result of the study of the effects of isothermal working conditions was that although differing microstructures could be obtained, in no circumstances were the coarse second-phase regions eliminated to the degree accomplished by Ness. This work eliminated the possibility of being able to design a satisfactory method of microstructural control using only isothermal working.

The effects of alloy chemistry were studied briefly. These experiments showed that Ness' success had not been dependent on some inadvertent addition of other alloy elements to the material. These results do not, however, mean that other alloy additions may not be beneficial in final optimization of microstructure to produce desired mechanical properties once the proper thermomechanical history has been developed.

The effect of thermal treatment alone was studied and showed that the microstructure demonstrated by Ness was not simply a result of variations in temperature. This study did show that it was possible to reduce considerably the number and size of the coarse second-phase regions by a scheme of thermal cycling. However, the development of a rather coarse precipitate structure also results from continued application of this treatment.

Finally, some attempt was made to combine both thermal treatment effects and mechanical deformation effects in a truly



thermomechanical scheme. Again, the coarse second-phase regions could not be eliminated. However, the precipitate structure which resulted was encouraging. The implication of this experiment was that combined treatment schemes of some sort would be required in these alloys.

It was intended at the beginning of this research to work with alloy compositions well into the two-phase region of the phase diagram. This intention was based on the demonstrated tendency for these alloys to evidence increasingly superplastic behavior as magnesium content is increased. It was realized that increased magnesium content also leads to much larger volume fractions of the brittle  $\beta$  phase, resulting in a loss of ductility at ambient temperatures. Were it possible, however, to overcome this brittleness through thermomechanical processing, no matter how complex, it was felt the added property of superplasticity would be well worth any extra effort necessary in processing. It was also thought during the earlier stages of research that the mechanism of Ness' success was one of breaking-up the  $\beta$  regions and distributing the resulting fine particles throughout the matrix. It is evident now, as a result of this research, that Ness was probably instead working the material as precipitation was occurring in the matrix.

The fact that Ness may have been working with a magnesium content well below that indicated by the nominal composition of the alloy is significant when coupled with the theory of



deformation controlled precipitation. Figure 37 illustrates the great reduction in the volume fraction of the  $\beta$  phase which is possible by giving up only 4% magnesium. This graph shows that a 15% Mg alloy can be given a soaking treatment at 430°C which would reduce the  $\beta$  phase volume fraction to about 0.1. The best result which could be expected from a 19% Mg alloy under this treatment is a reduction to about 0.3. Also important here is the realization that the cast structure in these alloys is a non-equilibrium structure exhibiting more  $\beta$  phase than predicted by the phase diagram and less magnesium dissolved in the solid solution matrix. Thus a soaking treatment would lead to even more effective reduction of the  $\beta$  phase from the cast alloy than that expected from an equilibrium microstructure.

The equilibrium phase diagram shows that the  $\beta$  phase can be eliminated completely by this high temperature soaking treatment if magnesium content is below 15%. This leads to a possible treatment scheme for alloys containing somewhat less than 15% Mg. After casting, the alloy would be solution treated in the single-phase aluminum-magnesium solid solution region, and then cooled at a rapid enough rate to minimize precipitation of the  $\beta$  phase. Subsequently the alloy would be reheated to a temperature in the two-phase region and isothermally worked by forging or rolling to control precipitation and refine the solid solution matrix structure simultaneously.



The ability to somewhat break-up and refine the  $\beta$  phase was evidenced by the results of this research. Thus it is possible that this process can be extended to alloys with magnesium contents approaching 15%. Although all of the  $\beta$  would not be eliminated by the solutioning treatment, the small volume fraction remaining may exist in fine enough particles to be further refined through breaking-up during deformation.





## IX. CONCLUSIONS AND RECOMMENDATIONS

It has been shown in this research that the development of an aluminum-magnesium alloy possessing excellent ambient temperature properties as well as being superplastic at elevated temperatures may not be possible. There appears to be a trade-off necessary between processability, formability and ambient temperature properties. This is brought about by the inability to eliminate the coarse  $\beta$  phase from the microstructure in alloys with magnesium contents greater than or equal to 15%, which alloys tend more toward superplastic mechanical behavior as magnesium content is increased. However, it is possible that an alloy containing less than 15% Mg could be processed in a manner which would result in a microstructure indicative of good ambient temperature properties coupled with good formability if not near superplasticity at elevated temperatures.

Work being conducted subsequent to this research is showing that an alloy of Al-15Mg can be processed using the high temperature soaking treatment followed by forging at a somewhat lower temperature and results in a fine two-phase microstructure exhibiting little coarse  $\beta$  phase remaining from the casting. With the exception of very small amounts of coarser  $\beta$ , the microstructures are very similar to those demonstrated by Ness.

It is highly recommended that research be continued in this area. The process of soaking or solution treating followed by



isothermal deformation at various temperatures needs to be investigated completely for alloys with magnesium contents ranging from 10% to 15% by weight. The resulting microstructures, as well as mechanical properties, must be examined to determine the best combination of properties attainable using this process.

It must also be determined with more accuracy what the alloy composition was of Ness' material. Wet chemistry methods will be required to determine accurately magnesium content in these materials. If it is determined that Ness was successful in processing an alloy with greater than 15% magnesium, attention must be given to the one aspect of Ness' process not duplicated in this research. This is the higher strain rates involved in rolling, which may be as much as two orders of magnitude higher than those used in the forging operations conducted during this research. Application of a process of successive light, hot deformations at strain rates as high as 5 per second after a high temperature soaking treatment may be the key to processing alloys above 15% Mg.

In any event, the ultimate goal of developing an alloy representing an increase in strength to weight ratio over current alloys is still valid and perhaps a bit closer to reality as a result of this research. The Navy of the future will require new ships and aircraft, and these could benefit in both performance and capability by the use of such an alloy.



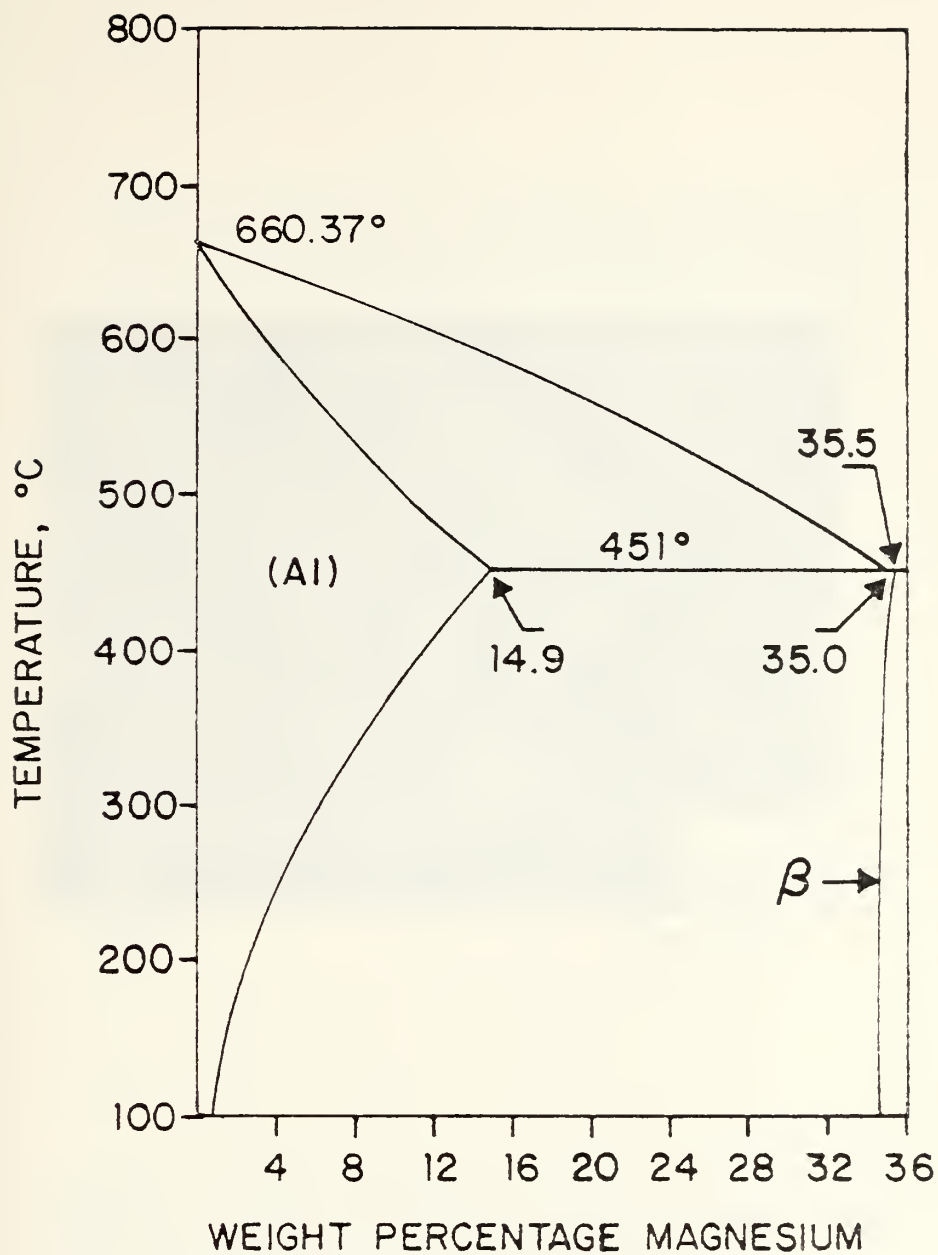
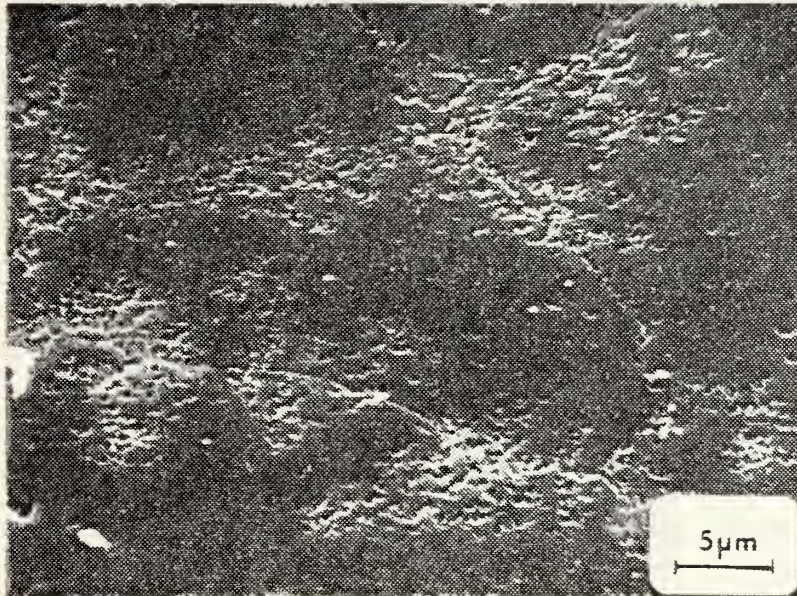


Figure 1 - Equilibrium phase diagram of the aluminum-magnesium binary system showing the aluminum rich portion to 36% magnesium by weight. Adapted from Ref. [1].







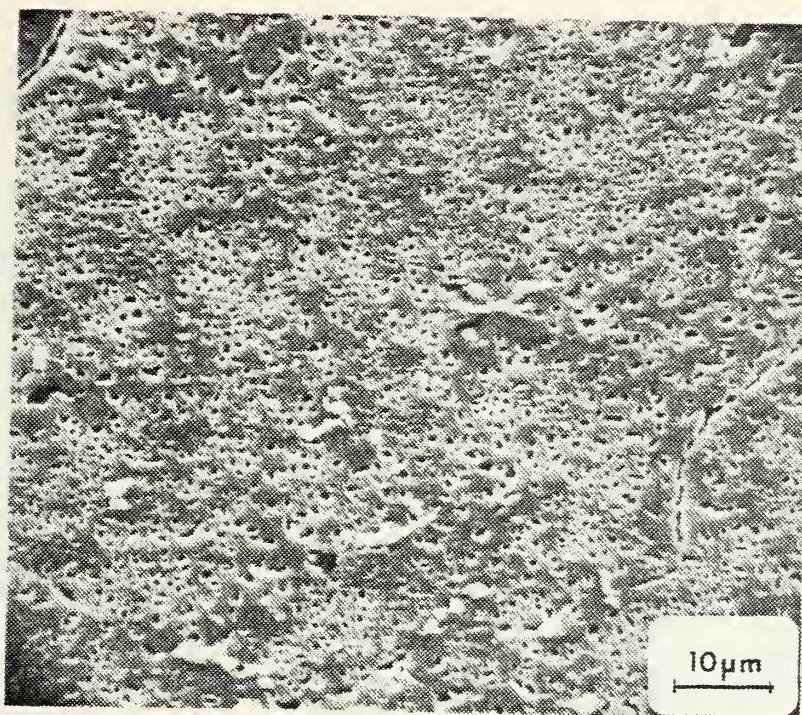
2550X

HF etch

Figure 2 - SEM photomicrograph showing the type of microstructure achieved by Ness in warm rolling of an Al-18Mg alloy. From Ness [5].







1225X

HF etch

Figure 3 - SEM photomicrograph of a nominally Al-18Mg alloy showing final results of Ness' work. Black areas are  $\beta$  intermetallic precipitates, gray areas are Al-Mg solid solution matrix. From Ness [5].



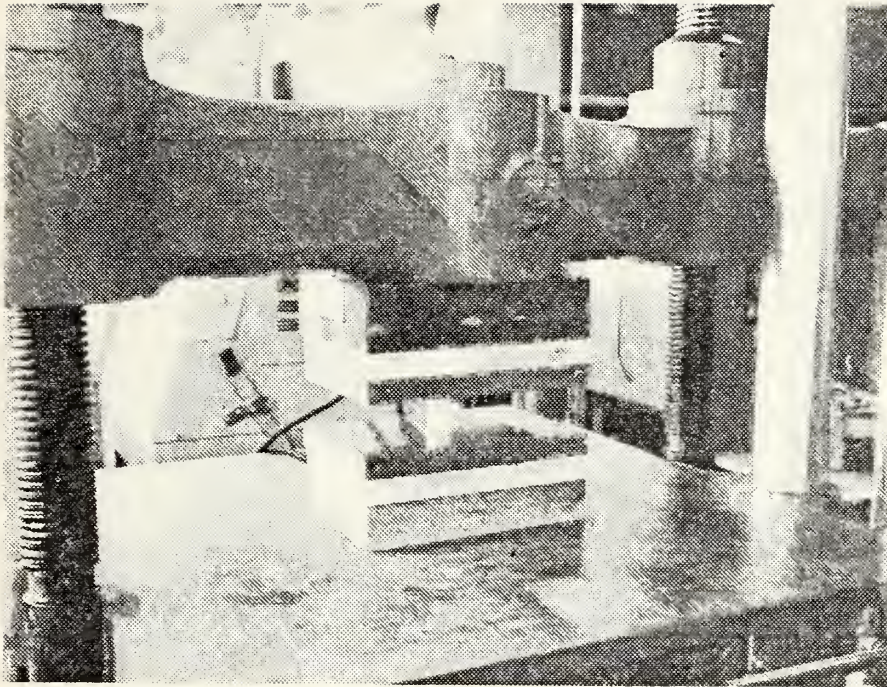
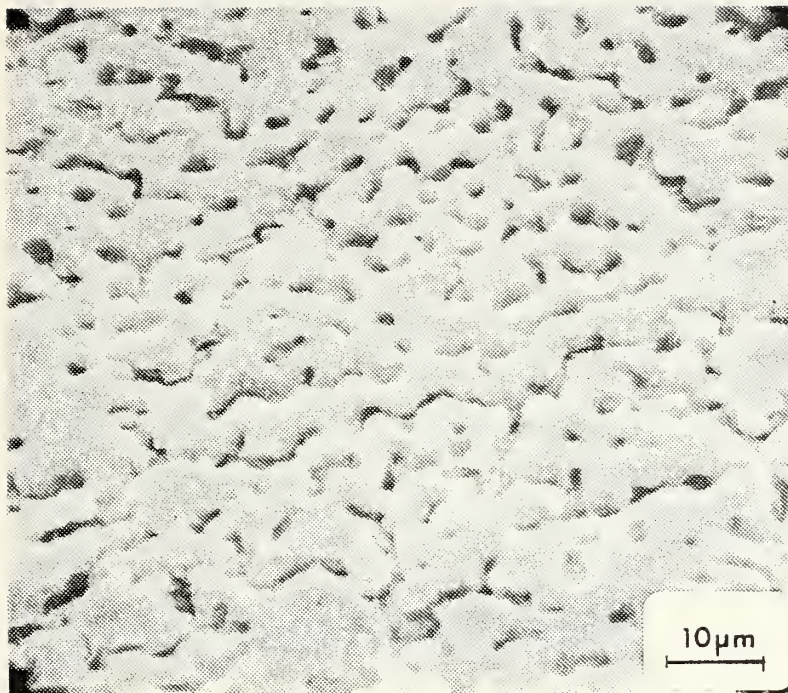


Figure 4 - Baldwin - Tate - Emery testing machine modified for hot forging operations. Upset forging billet in forging position on heated platens.





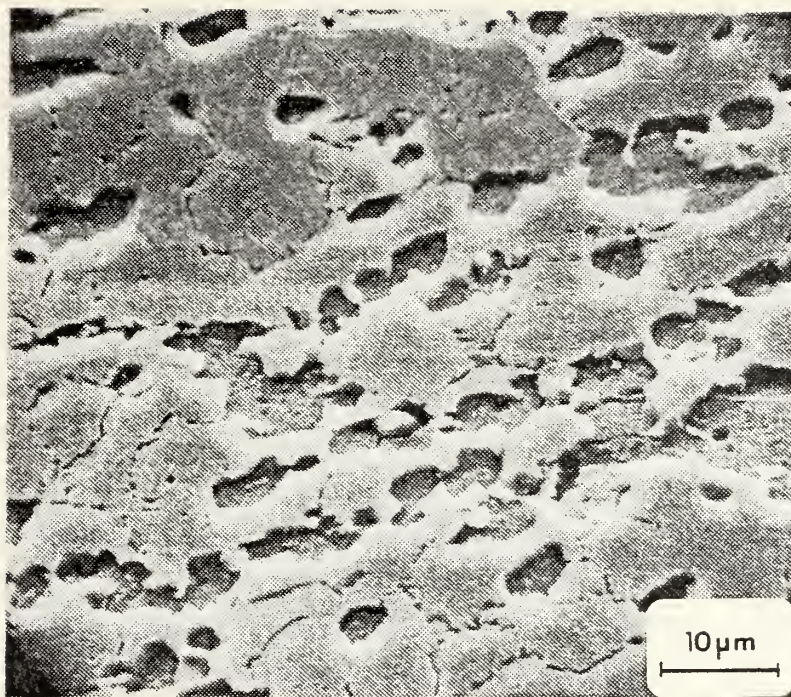


1270X

H<sub>3</sub>PO<sub>4</sub> etch

Figure 5 - SEM photomicrograph showing microstructure of Al-18Mg casting.





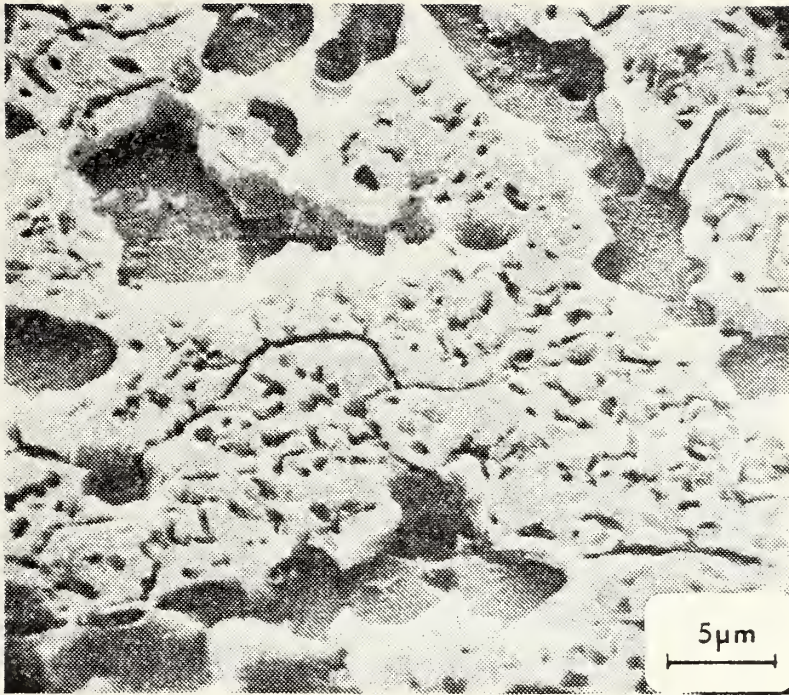
1490X

$\text{H}_3\text{PO}_4$  etch

Figure 6 - SEM photomicrograph of Al-18Mg alloy after isothermal forging at 400°C to a strain of 2.0. Sample was given a 20-hour soak at 400°C prior to deformation.





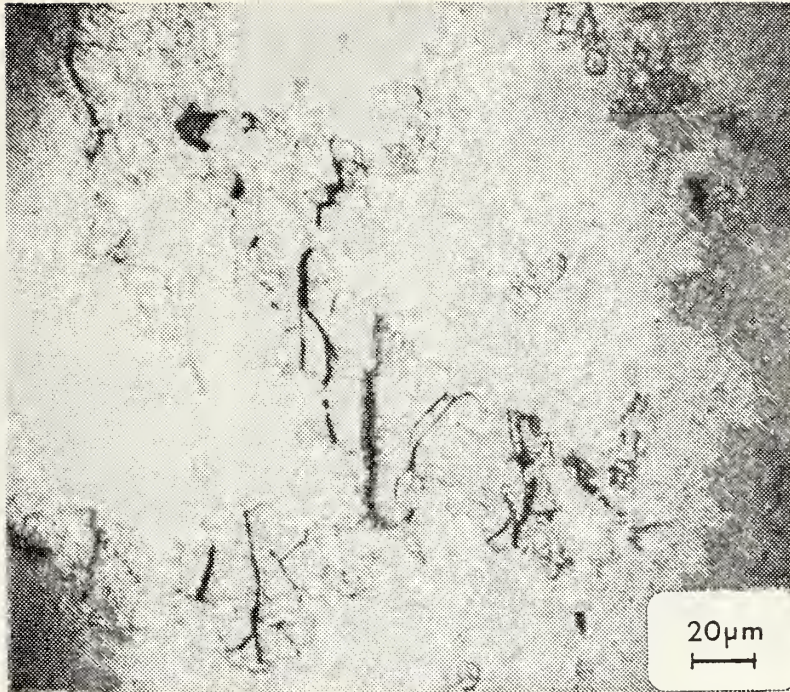


2850X

$\text{H}_3\text{PO}_4$  etch

Figure 7 - SEM photomicrograph of Al-18Mg alloy after hot rolling 10% at 300°C.





400X

HF etch

Figure 8 - Light photomicrograph of Al-18Mg alloy showing cracks in  $\beta$  intermetallic particles as a result of deformation processing.





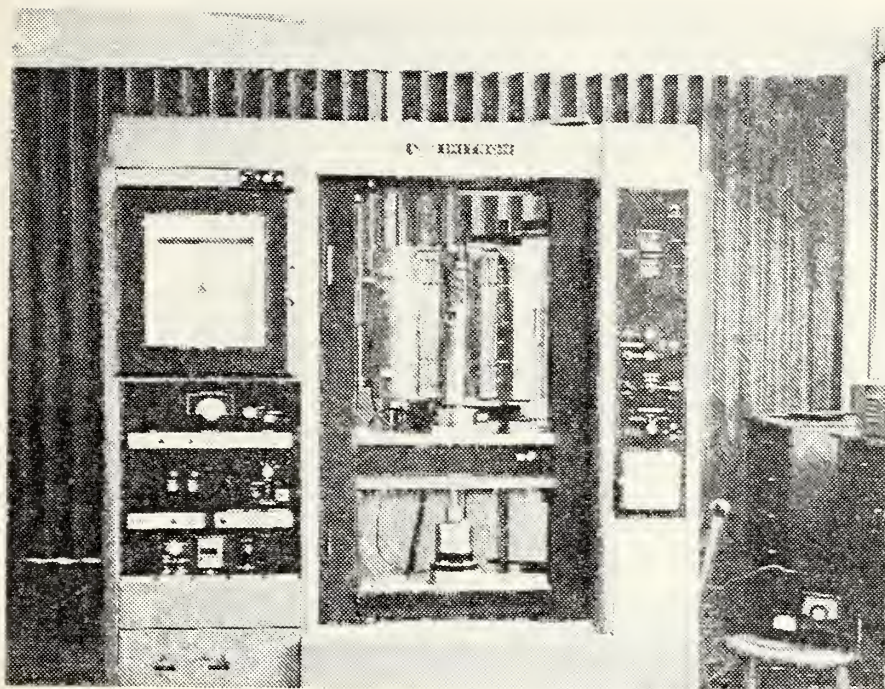


Figure 9 - Instron testing machine modified for hot, isothermal compression testing.



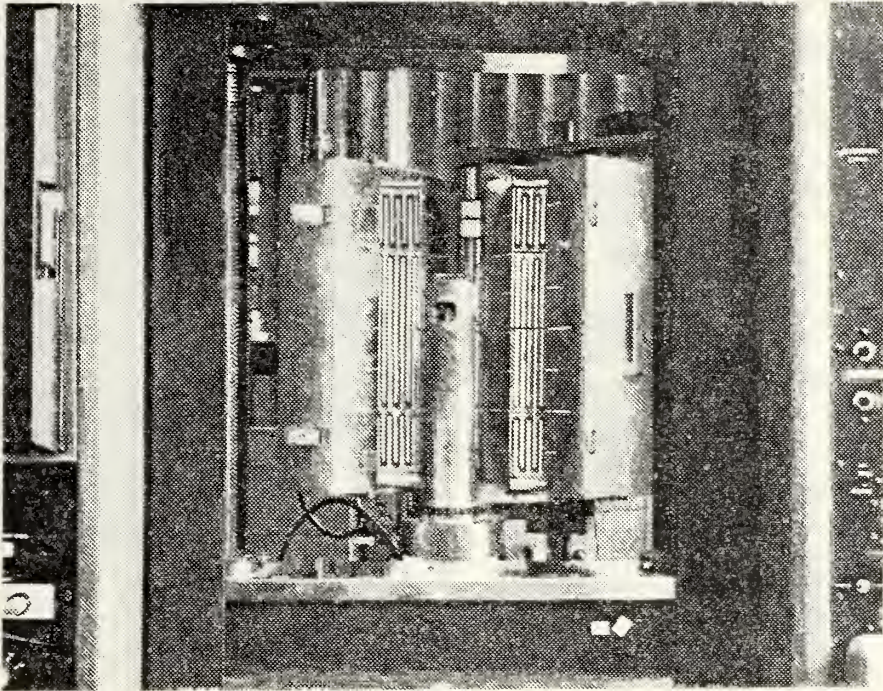
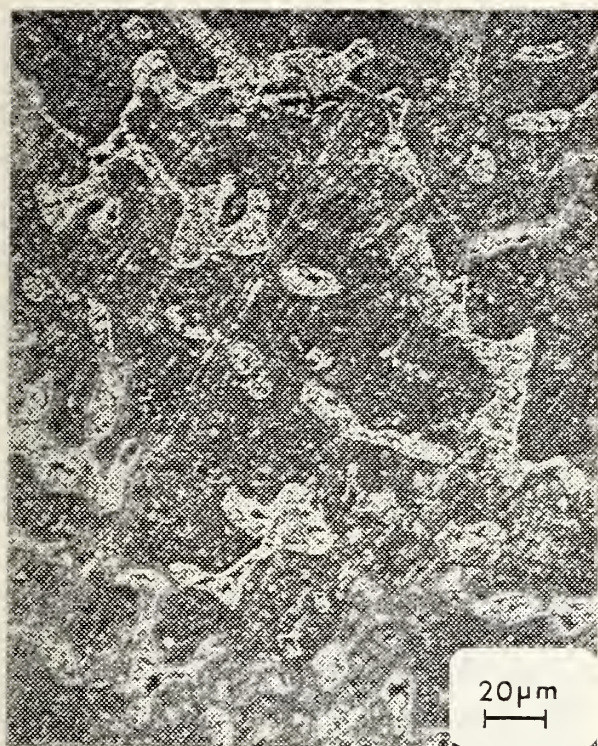


Figure 10- Marshall split furnace opened  
to expose test chamber.







400X

HF etch

Figure 11 - Light photomicrograph showing the cast structure of VEX0219-2 (Al-15Mg). White areas are  $\beta$  intermetallic; black areas are Al-Mg solid solution matrix.

400X

HF etch

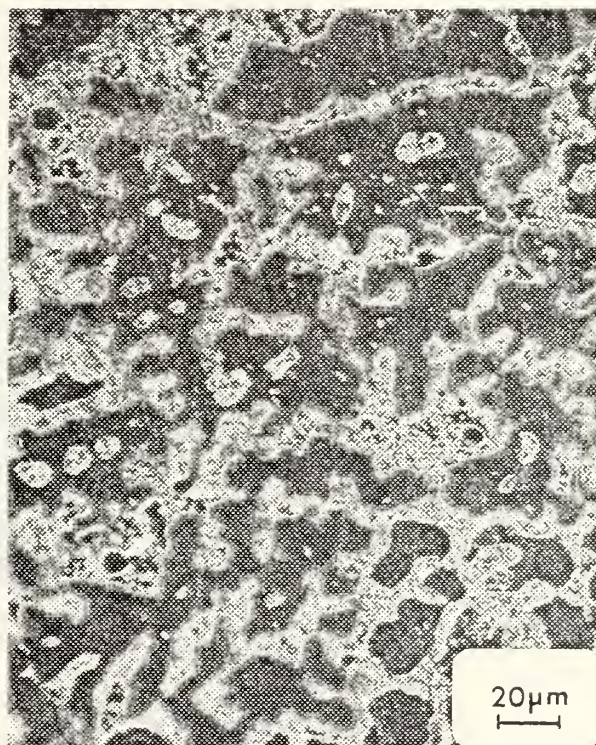


Figure 12 - Light photomicrograph showing the cast structure of VEX0219-3 (Al-19Mg). White areas are  $\beta$  intermetallic; black areas are Al-Mg solid solution matrix.





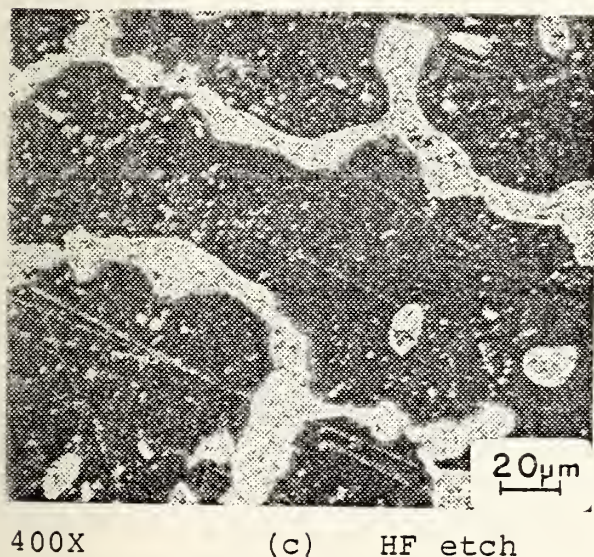
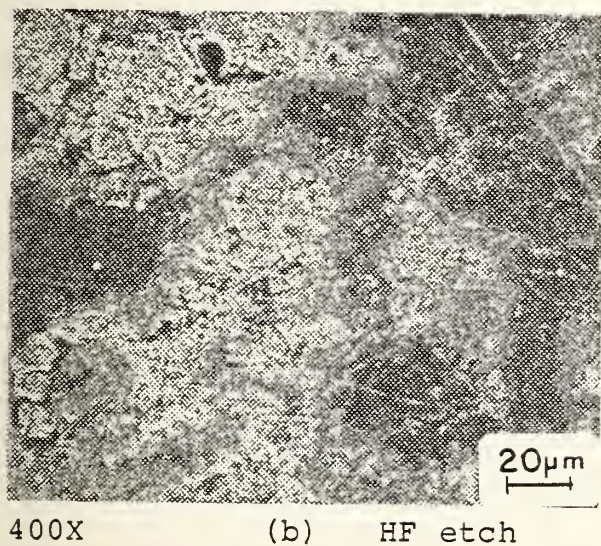
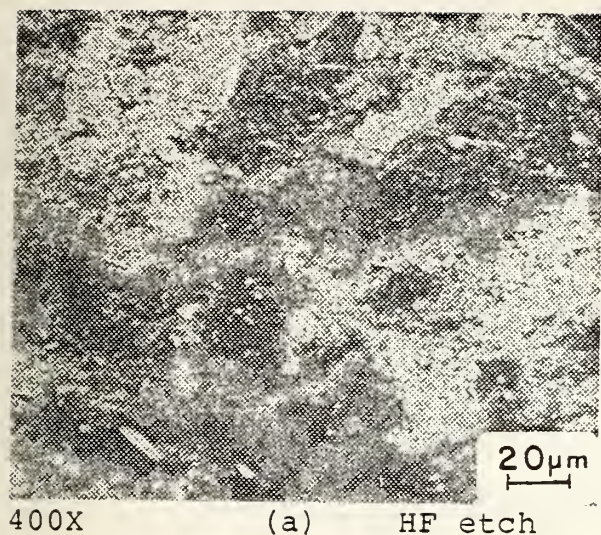


Figure 13 - Light photomicrographs of VEX0219-2 (Al-15Mg) showing the effect of isothermal compression testing at various temperatures to a strain of 1.5 at a strain rate of  $10^{-3}\text{sec}^{-1}$ . Light areas are  $\beta$  intermetallic; dark areas are Al-Mg solid solution matrix.

(a) Sample 39, 200°C

(b) Sample 48, 270°C

(c) Sample 57, 415°C



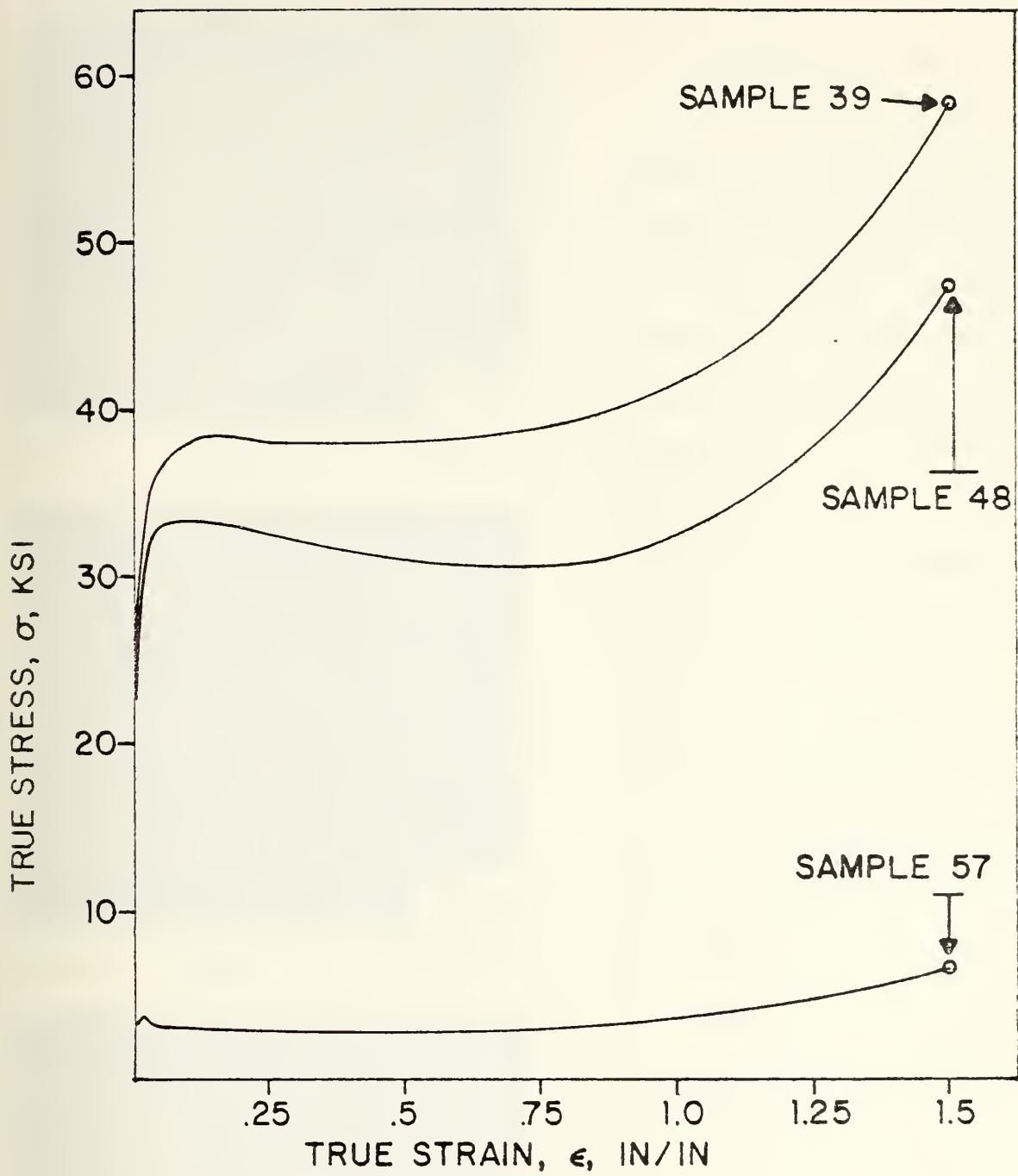
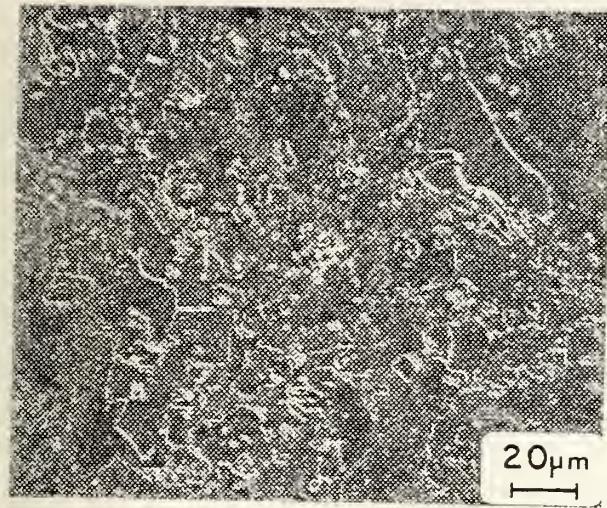


Figure 14 - Compressive stress-strain curves for samples in Figure 13.



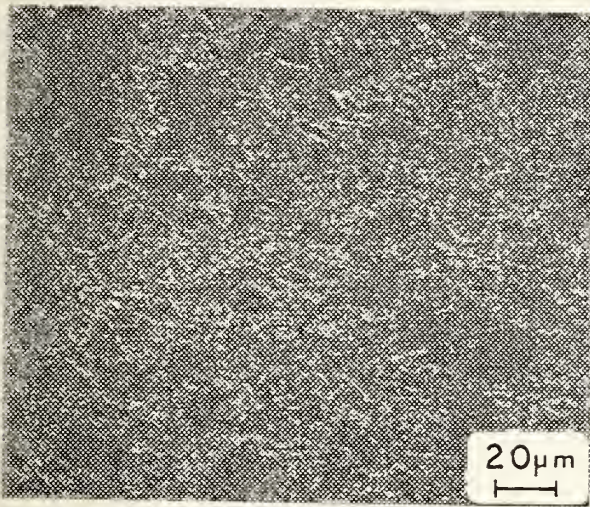




400X

(a)

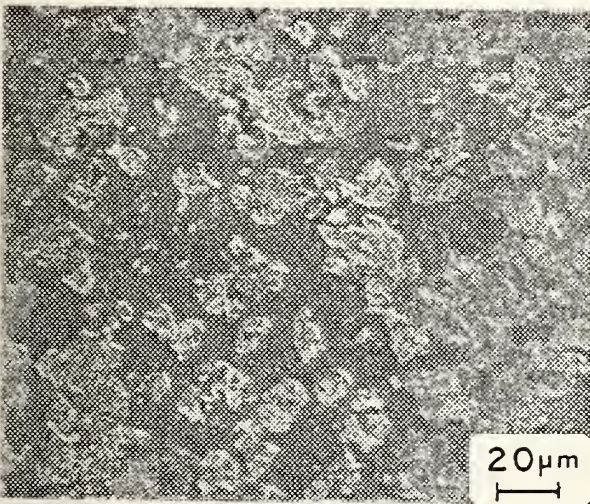
HF etch



400X

(b)

HF etch



400X

(c)

HF etch

Figure 15 - Light photomicrographs of VEX0219-3 (Al-19Mg) after isothermal compression testing at various temperatures to a strain of 1.5 at a strain rate of  $10^{-3}\text{sec}^{-1}$ . Light features are  $\beta$  intermetallic; dark or gray areas are Al-Mg solid solution matrix. Sharp white boundary features in (a) and (b) show outlines of coarse  $\beta$  particles remaining from the casting.

(a) Sample 69, 200°C

(b) Sample 78, 270°C

(c) Sample 87, 415°C





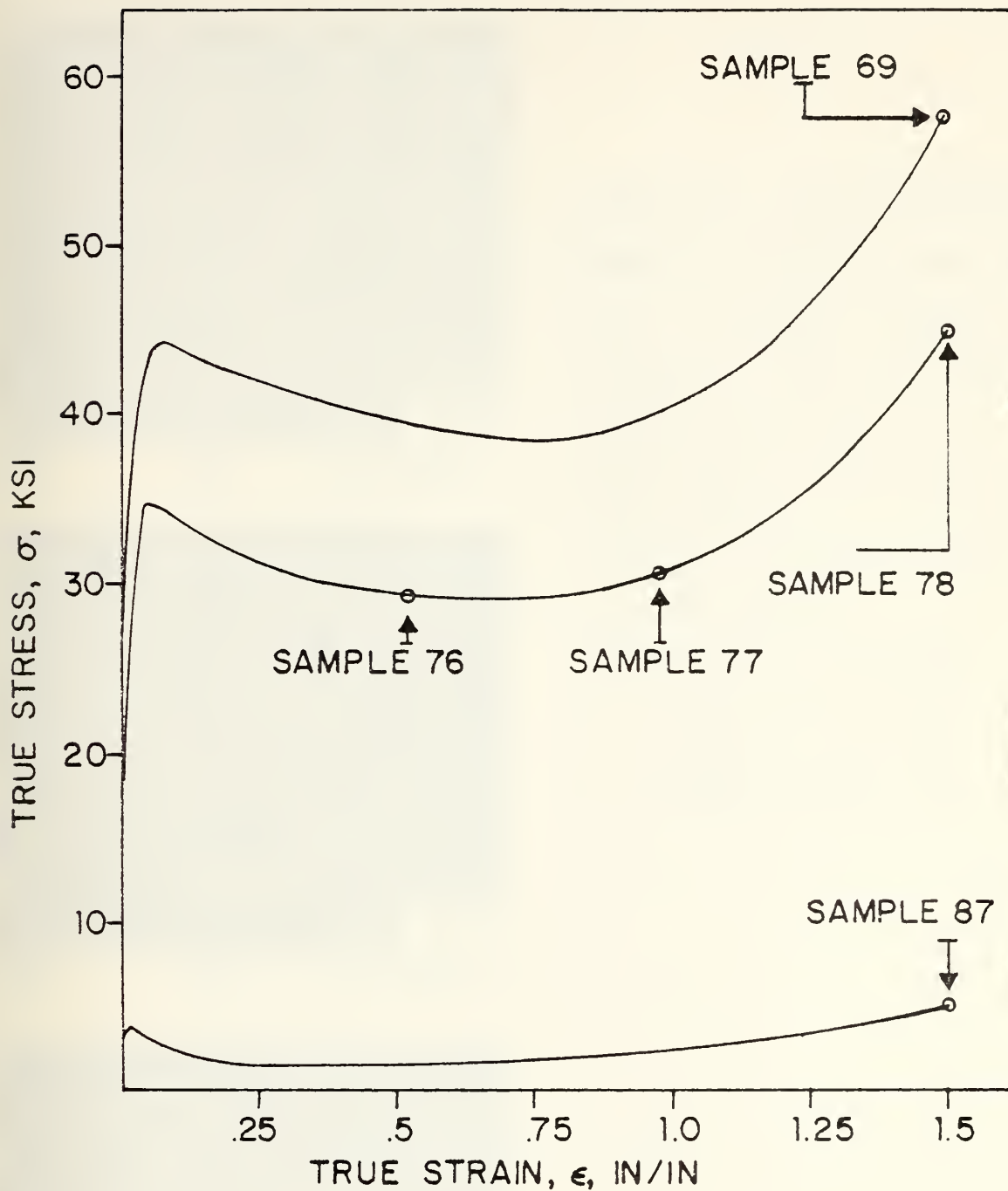
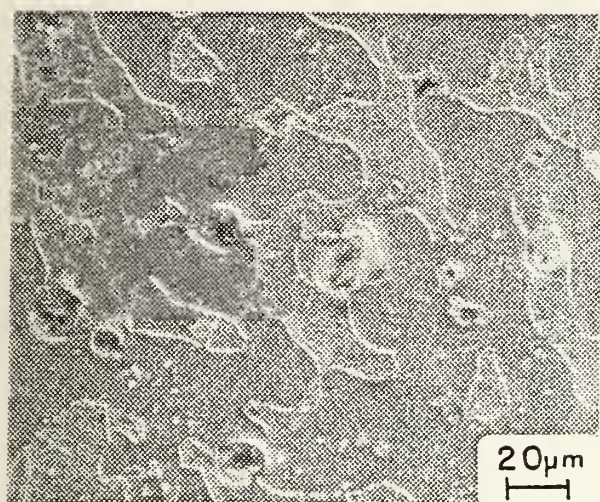
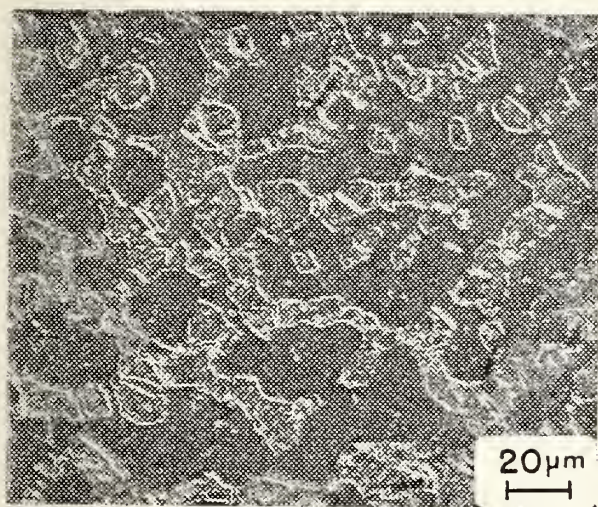


Figure 16 - Compressive stress-strain curves showing the relative flow stress levels of samples in Figures 15 and 17.

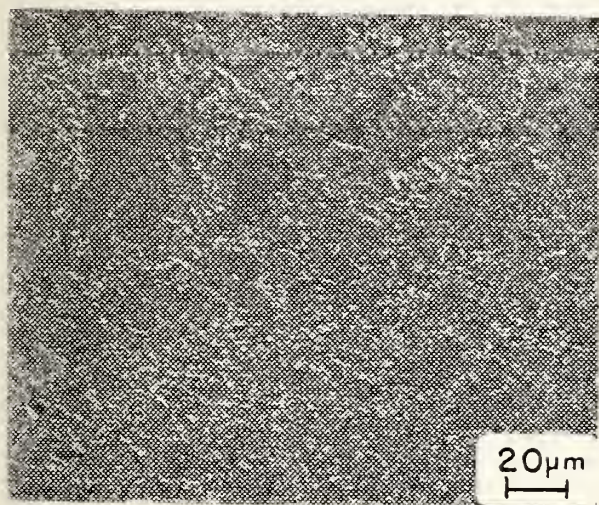




400X (a) HF etch



400X (b) HF etch



400X (c) HF etch

Figure 17 - Light photomicrographs of VEX0219-3 (Al-19Mg) after isothermal compression testing at 270°C and a strain rate of  $5 \times 10^{-3} \text{ sec}^{-1}$ .

17(a) through 17(c) show the effect of increasing strain on microstructure.

(a) Sample 76,  $\epsilon = 0.5$

(b) Sample 77,  $\epsilon = 1.0$

(c) Sample 78,  $\epsilon = 1.5$





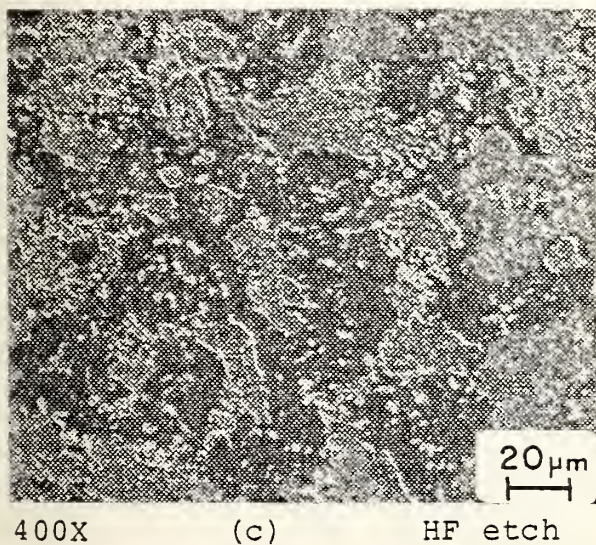
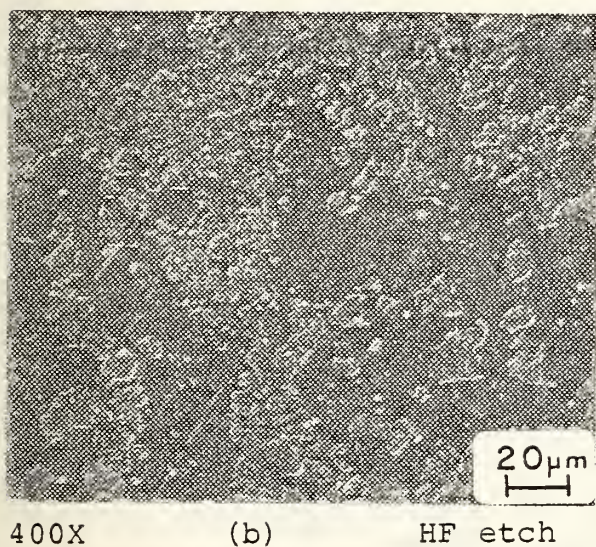
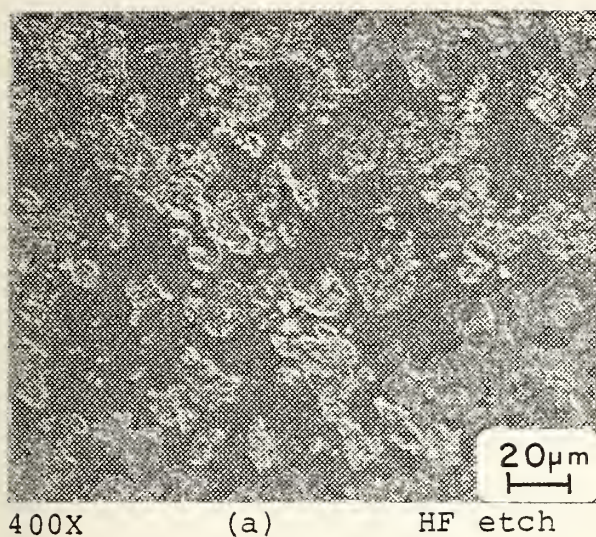


Figure 18 - Light photomicrographs of VEX0219-3 (Al-19Mg) after isothermal compression testing at 415°C to a strain of 1.5 showing the effect of decreasing strain rate on microstructure.

- (a) Sample 87,  
 $\dot{\epsilon} = 2 \times 10^{-2} \text{sec}^{-1}$
- (b) Sample 84,  
 $\dot{\epsilon} = 5 \times 10^{-3} \text{sec}^{-1}$
- (c) Sample 81,  
 $\dot{\epsilon} = 1 \times 10^{-3} \text{sec}^{-1}$



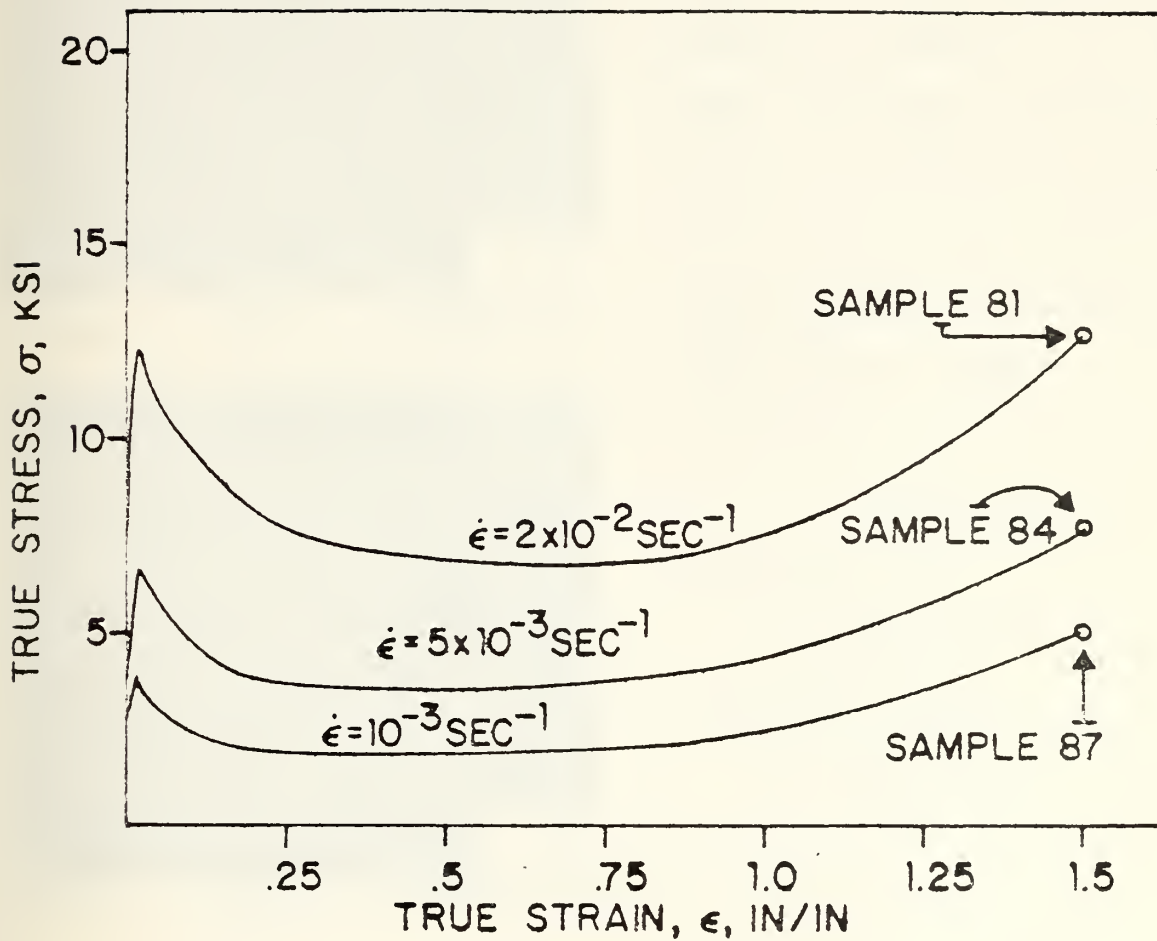
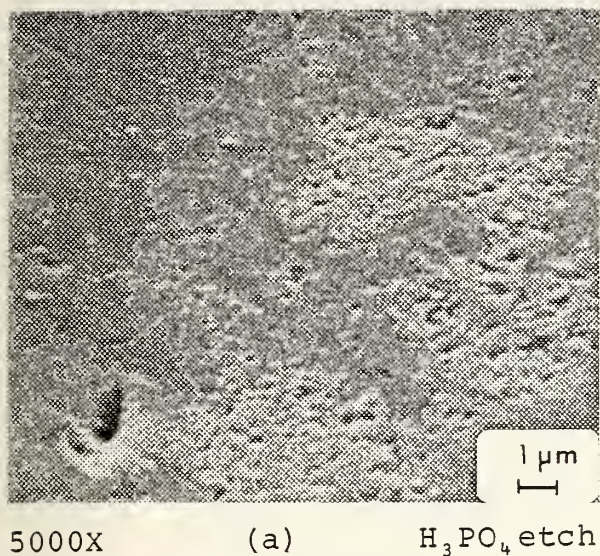


Figure 19 - Compressive stress-strain curves showing flow stress at various strain rates for samples of Figure 18.





Figure 20 - SEM photomicrographs of VEX0219-3 (Al-19Mg) after isothermal compression testing at 200°C to a strain of 1.5 showing the  $\beta$  precipitation structure resulting at three strain rates.



(a) Sample 63,

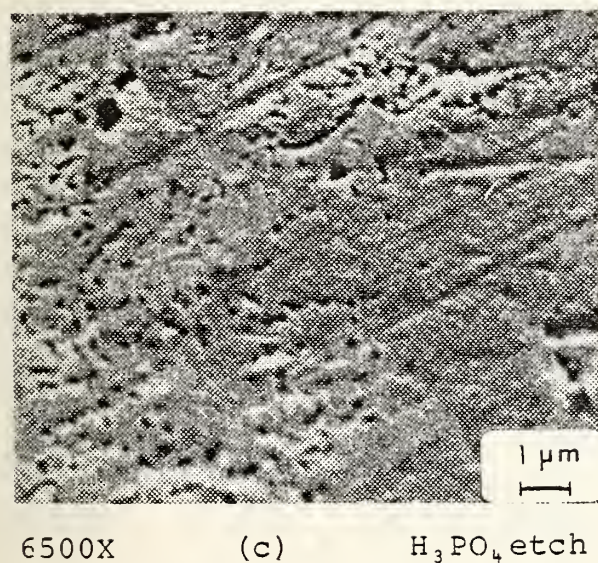
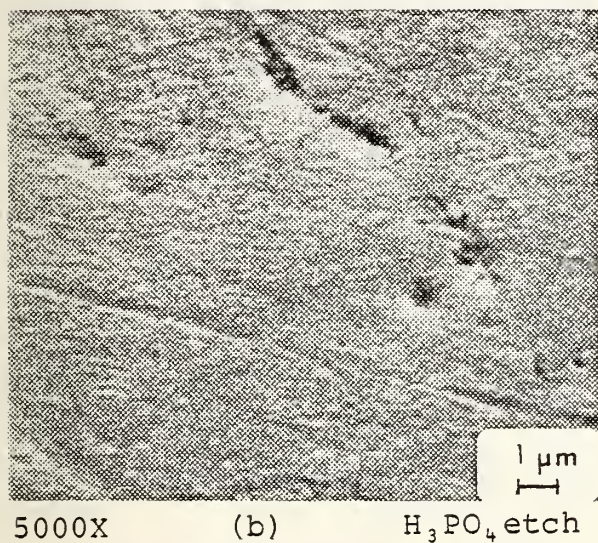
$$\dot{\epsilon} = 2 \times 10^{-2} \text{sec}^{-1}$$

(b) Sample 66,

$$\dot{\epsilon} = 5 \times 10^{-3} \text{sec}^{-1}$$

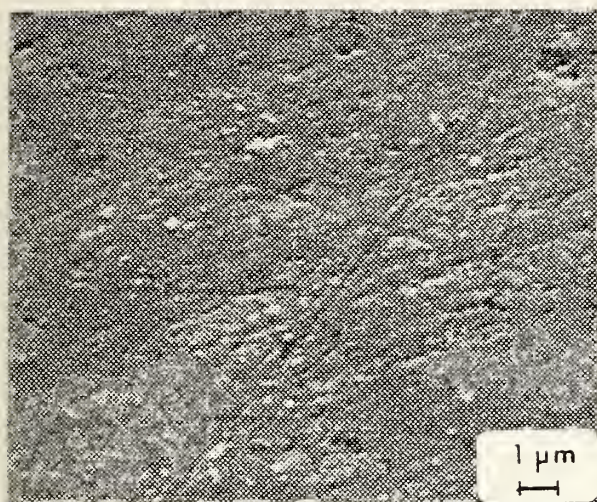
(c) Sample 69,

$$\dot{\epsilon} = 1 \times 10^{-3} \text{sec}^{-1}$$

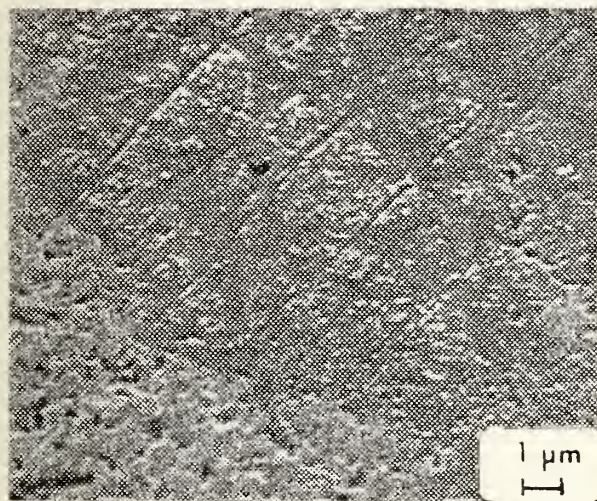




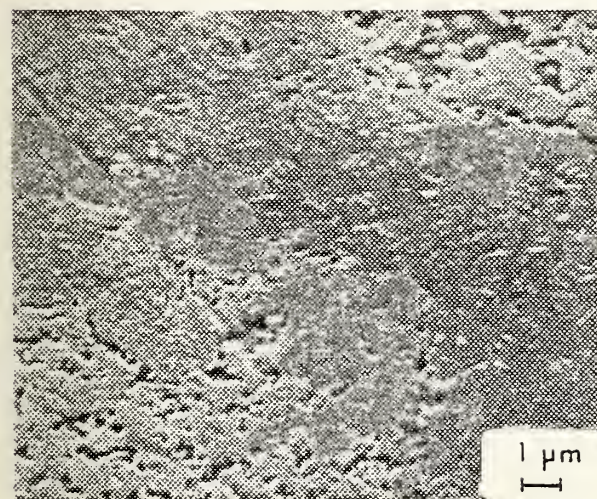




5000X (a)  $\text{H}_3\text{PO}_4$  etch



5000X (b)  $\text{H}_3\text{PO}_4$  etch



5000X (c)  $\text{H}_3\text{PO}_4$  etch

Figure 21 - SEM photomicrographs of VEX0219-3 (Al-19Mg) after isothermal compression testing at 270°C to a strain of 1.5, showing the  $\beta$  precipitation structure resulting at three strain rates.

(a) Sample 72,

$$\dot{\epsilon} = 2 \times 10^{-2} \text{sec}^{-1}$$

(b) Sample 75,

$$\dot{\epsilon} = 5 \times 10^{-3} \text{sec}^{-1}$$

(c) Sample 78,

$$\dot{\epsilon} = 1 \times 10^{-3} \text{sec}^{-1}$$





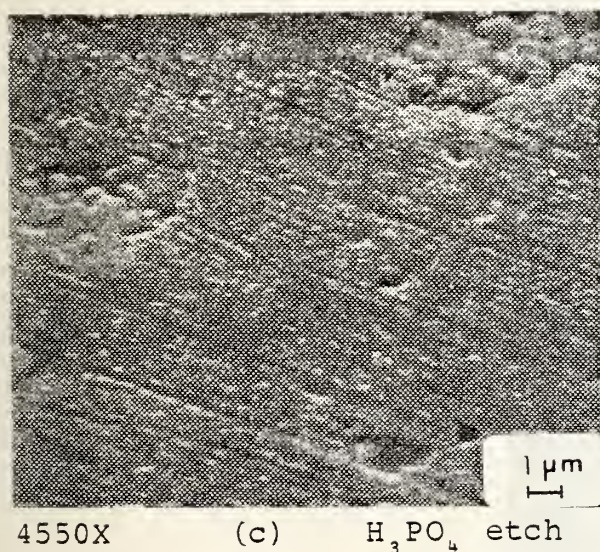
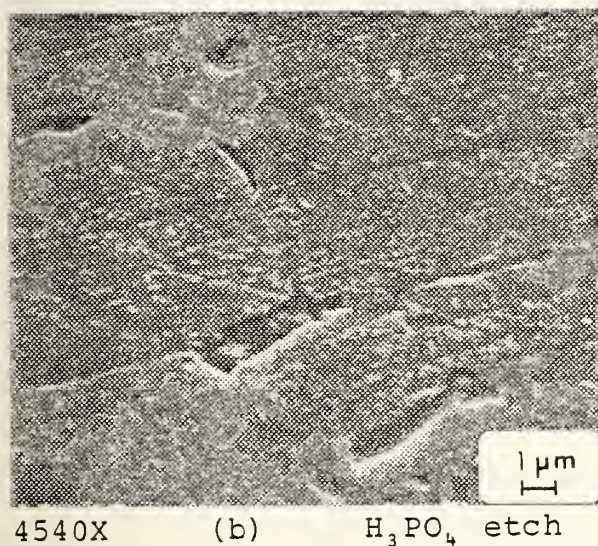
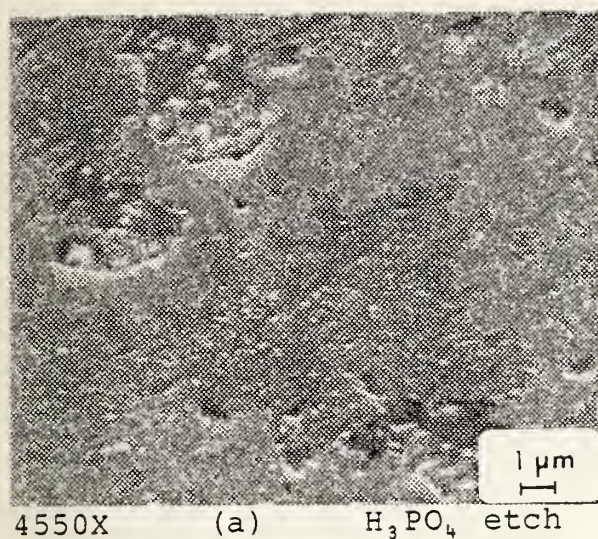


Figure 22 - SEM photomicrographs of VEX0219-3 (Al-19Mg) after isothermal compression testing at 415°C to a strain of 1.5, showing the  $\delta$  precipitation structure resulting at three strain rates.

(a) Sample 81,

$$\dot{\epsilon} = 2 \times 10^{-2} \text{sec}^{-1}$$

(b) Sample 84,

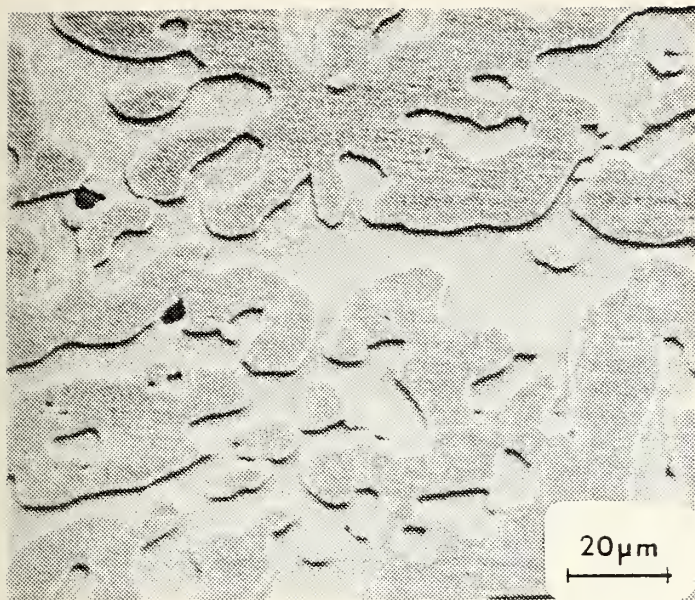
$$\dot{\epsilon} = 5 \times 10^{-3} \text{sec}^{-1}$$

(c) Sample 87,

$$\dot{\epsilon} = 1 \times 10^{-3} \text{sec}^{-1}$$







(a)

Cast structure  
before forging.

680X

$H_3PO_4$  etch

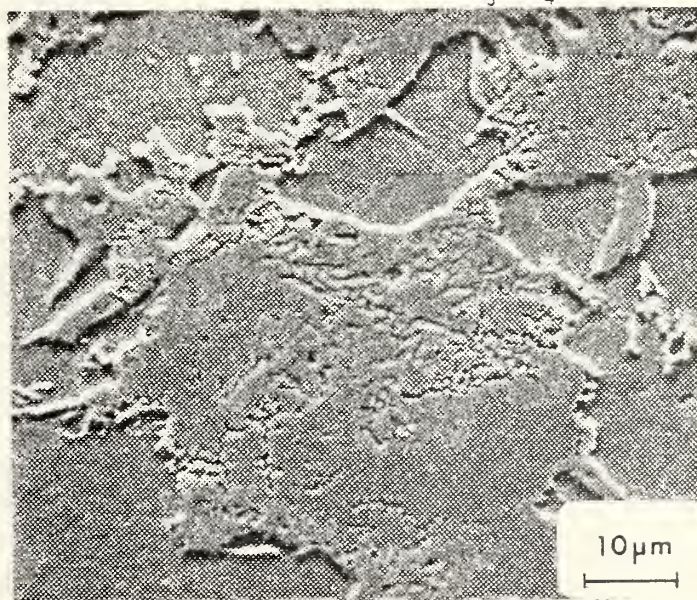
Figure 23 - SEM photomicrographs of VEX0219-3 (Al-19Mg) before and after isothermal forging. The raised areas are the Al-Mg solid solution matrix; the depressed areas are the  $\beta$  intermetallic phase.

1200X

$H_3PO_4$  etch

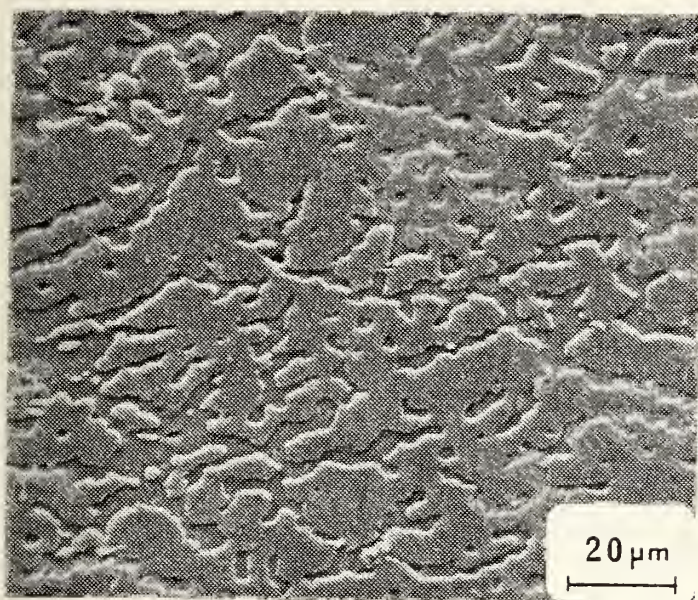
(b)

Structure after upset  
forging at 300°C to a  
strain of 1.6.









(a)

Cast structure  
before forging.

710X

$\text{H}_3\text{PO}_4$  etch

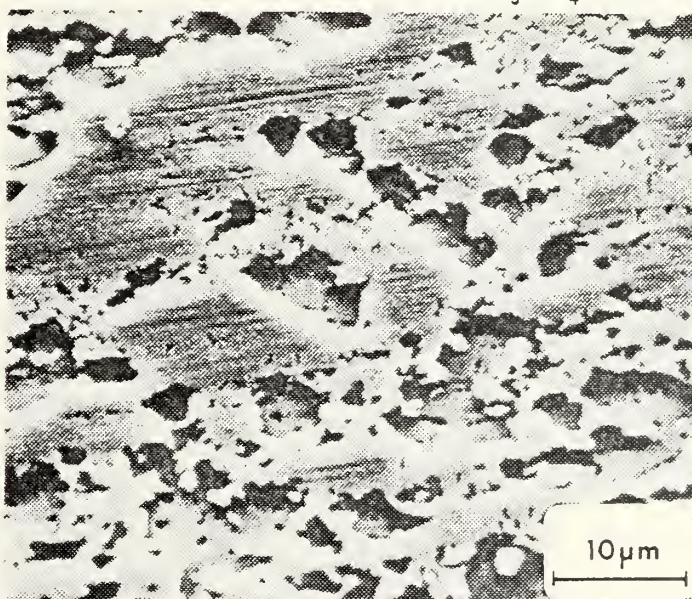
Figure 24 - SEM photomicrographs of Al-17.8Mg-0.3Fe alloy before and after isothermal forging. The coarse  $\beta$  phase has been refined but not eliminated in forging. From Glover [6].

(b)

Structure after upset  
forging at 300°C to a  
strain of 1.5.

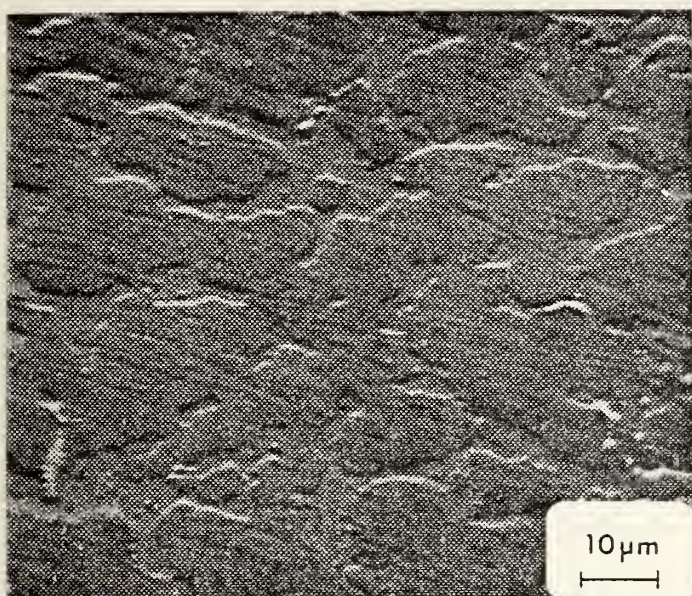
1700X

$\text{H}_3\text{PO}_4$  etch









1000X

$H_3PO_4$  etch

(a)

Cast structure  
before forging.

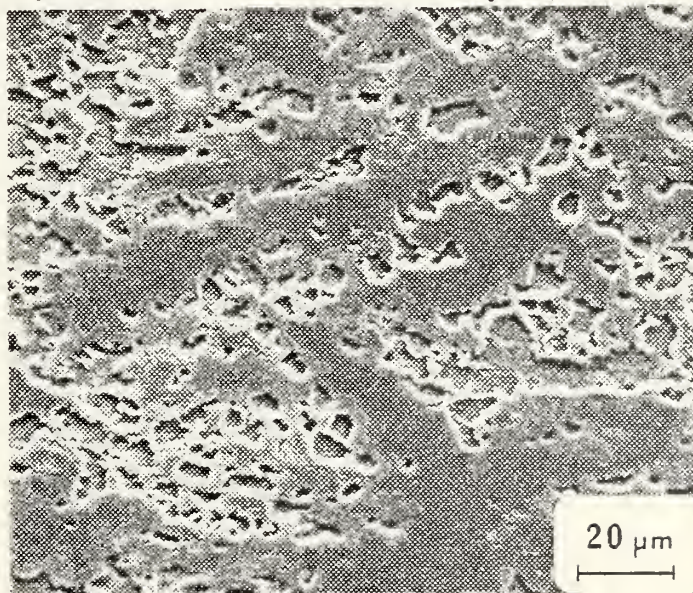
Figure 25 - SEM photomicrographs of Al-18Mg-0.5Zn alloy before and after isothermal forging. The  $\beta$  phase has been somewhat refined by forging but is still coarse.

640X

$H_3PO_4$  etch

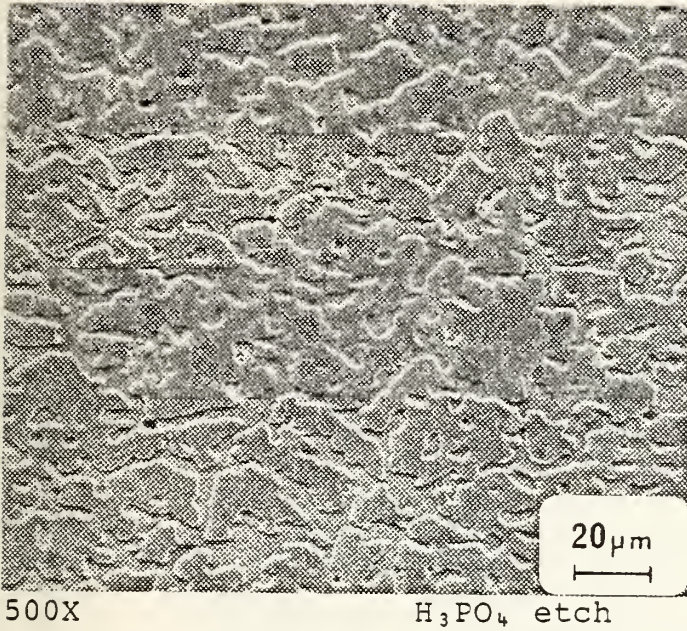
(b)

Structure after upset  
forging at 300°C to a  
strain of 1.4.







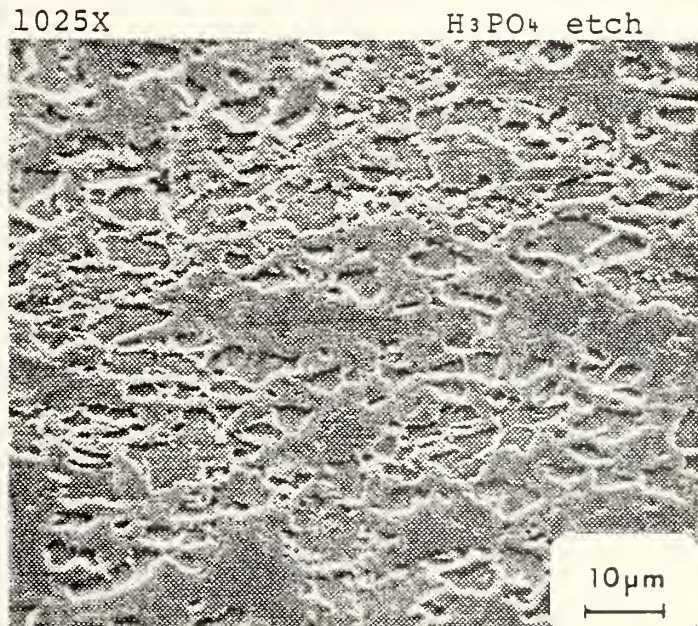


(a)  
Cast structure  
before forging.

Figure 26 - SEM photomicrographs of Al-19Mg-0.13Cu alloy before and after isothermal forging. Some refinement is evident after deformation, but the coarse  $\beta$  phase has not been eliminated.

(b)

Structure after upset  
forging at 300°C to a  
strain of 1.12.







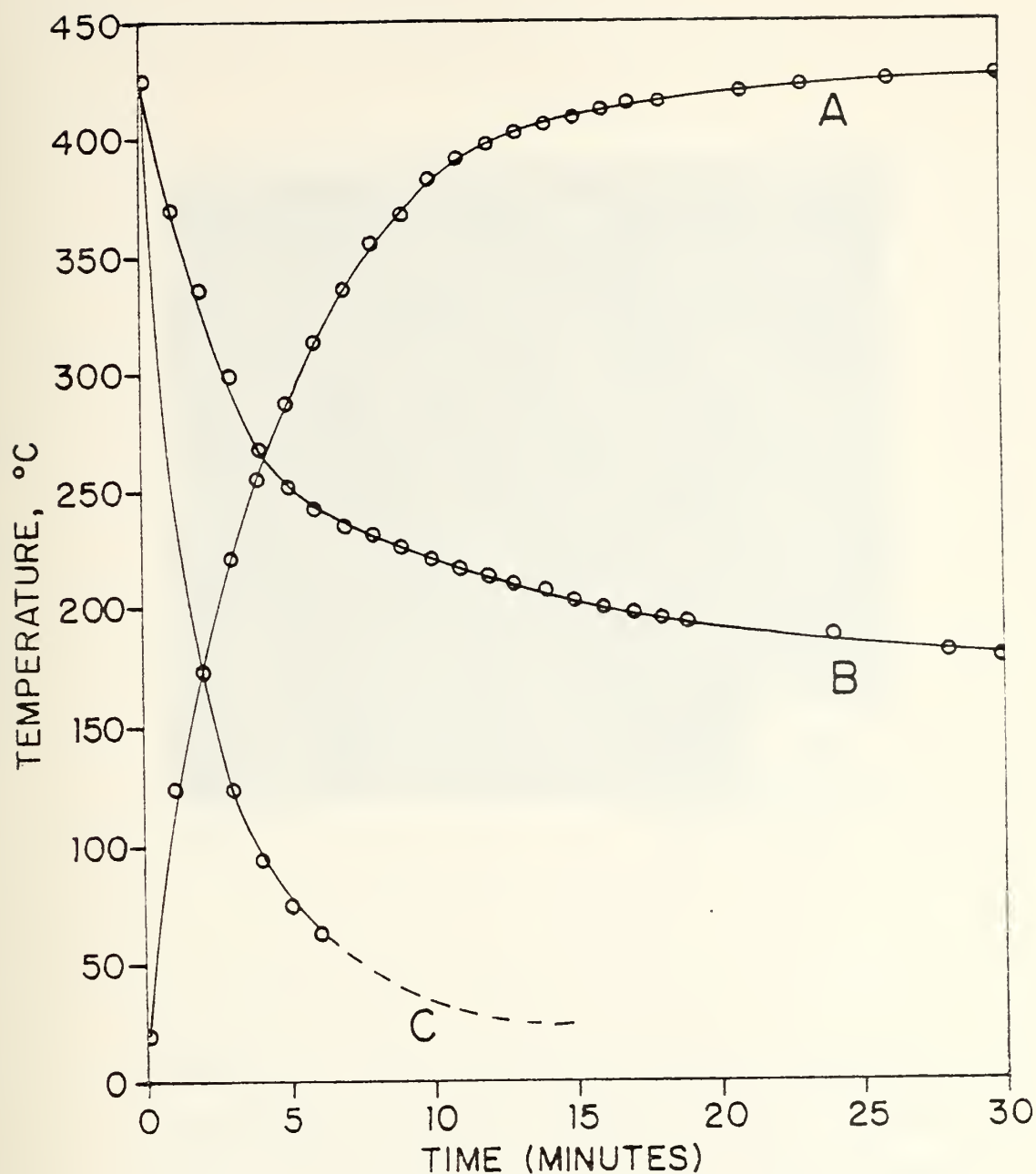
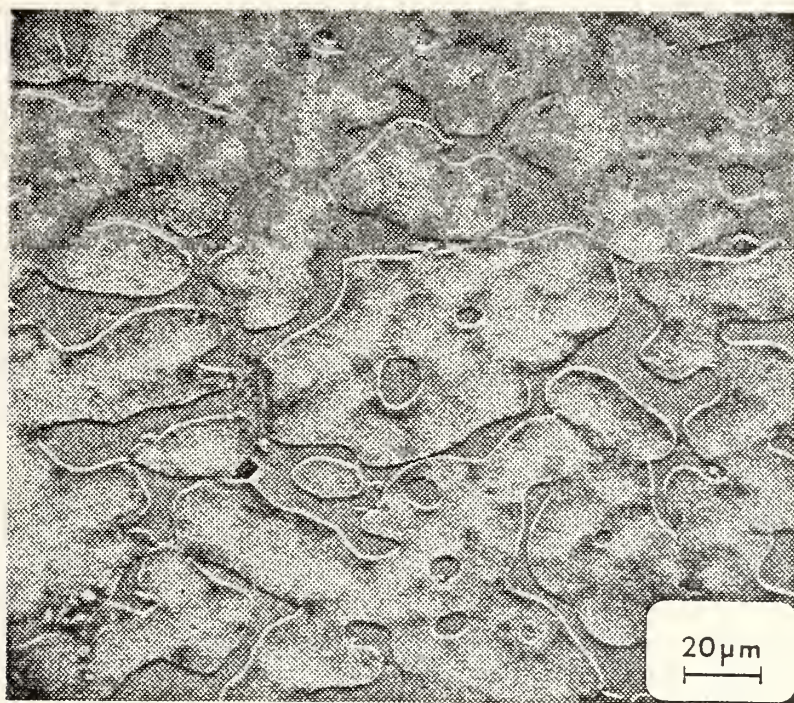


Figure 27 - Temperature vs time curves for Al-Mg alloys. Curve A is heating from room temperature to 425°C. Curve B is cooling from 425°C with the sample placed between two steel platens at 200°C. Curve C is cooling from 425°C by placing sample on steel plate at room temperature.





505X

$H_3PO_4$  etch

Figure 28 - SEM photomicrograph of VEX0219-3 (Al-19Mg) after being exposed to five temperature cycles, showing the overall microstructure. The recessed, solid gray areas are  $\beta$  phase remaining from the cast structure. This form of the  $\beta$  phase has not been eliminated but has been reduced. The variation in contrast within the Al-Mg solid solution (raised areas) indicate relative density of  $\beta$  precipitates, the lighter areas being more dense.





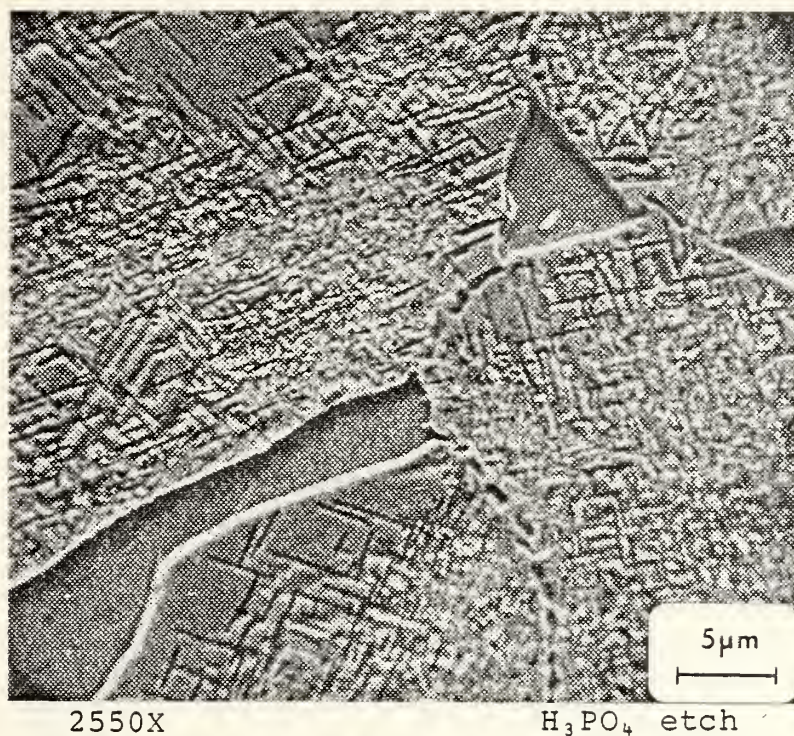


Figure 29 - SEM photomicrograph of VEX0219-3 (Al-19Mg) after being exposed to five temperature cycles, showing the precipitate structure. The linear features are Widmannstätten plates of  $\beta$  phase formed when the Mg is driven out of solution in the Al at the lower temperature half cycle. Parts of four grains of the Al-Mg solid solution matrix are visible as indicated by the different orientations of the precipitate plates. Grain boundary precipitates of  $\beta$  are also visible.





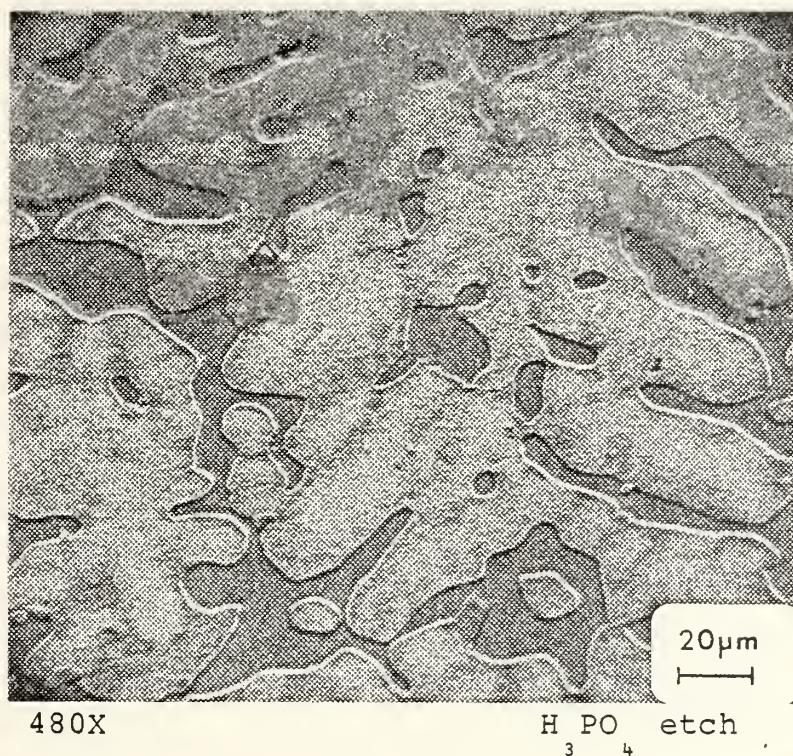


Figure 30 - SEM photomicrograph of VEX0219-3 (Al-19Mg) exposed to ten thermal cycles, showing the overall microstructure. The coarse  $\beta$  has been reduced in size but not eliminated. The precipitation structure is more homogeneous as indicated by the more uniform contrast in the raised areas.



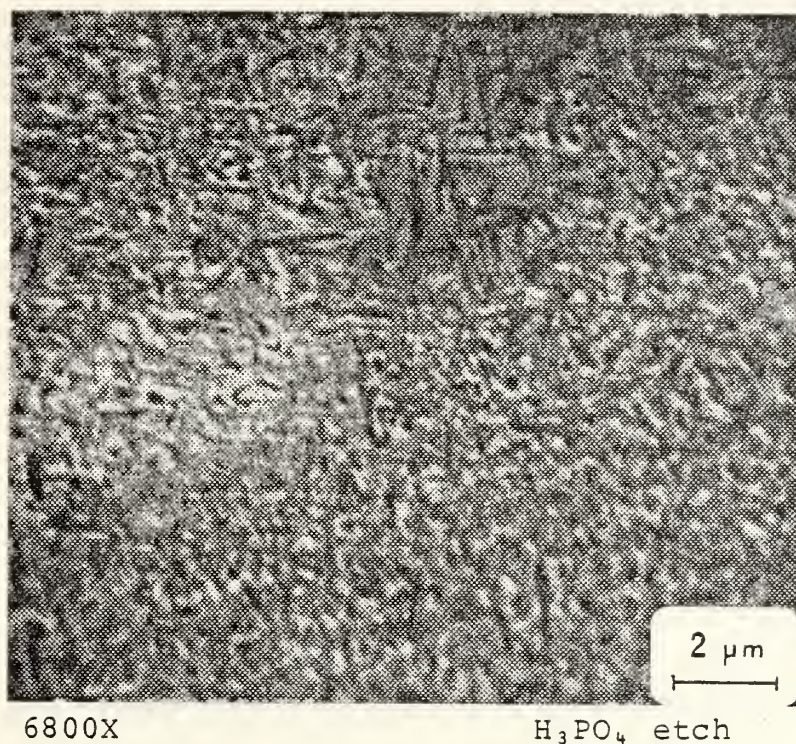
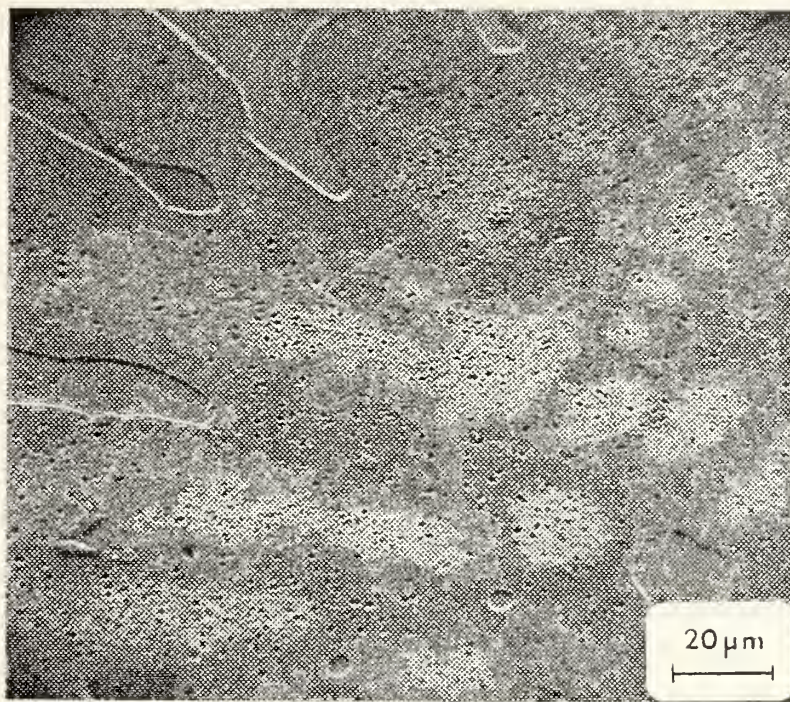


Figure 31 - SEM photomicrograph of VEX0219-3 (Al-19Mg) exposed to ten thermal cycles, showing the precipitate structure. The Widmannstatten precipitate structure is still visible but has largely been replaced by a more equiaxed, homogeneous precipitate structure made up of submicron sized particles.







650X

H<sub>3</sub>PO<sub>4</sub> etch

Figure 32 - SEM photomicrograph of VEX0219-3 (Al-19Mg) exposed to 15 thermal cycles, showing the overall microstructure. The coarse  $\beta$  from the cast structure has been further reduced in size, and a coarser precipitate structure is evident within the Al-Mg solid solution. The light areas are regions of dense smaller precipitates.





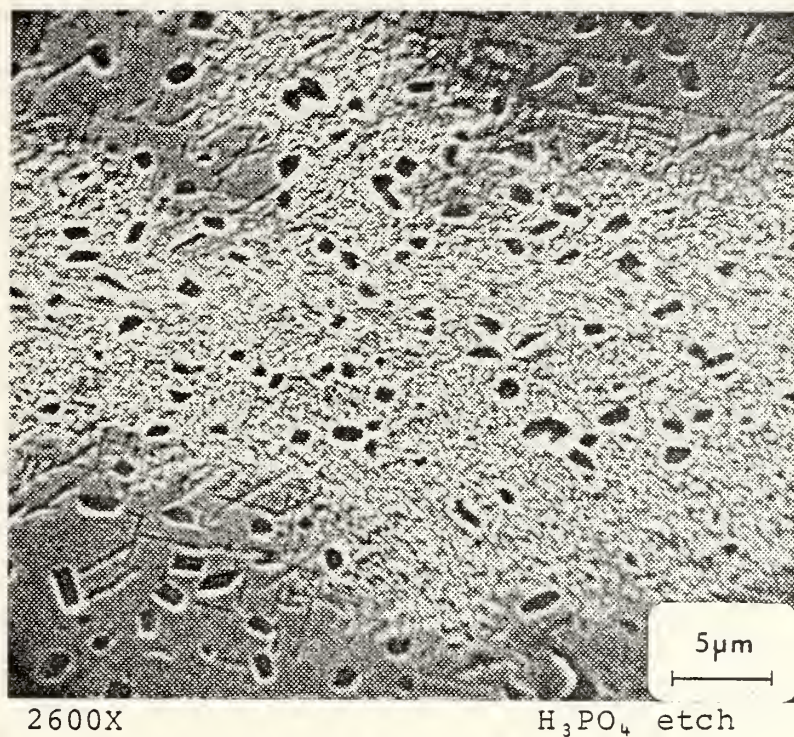


Figure 33 - SEM photomicrograph of VEX0219-3 (Al-19Mg) exposed to 15 thermal cycles, showing the precipitate structure. The larger precipitate particles which have formed between ten and fifteen cycles appear very angular indicating they have grown from the Widmannstatten structure formed earlier in the process.



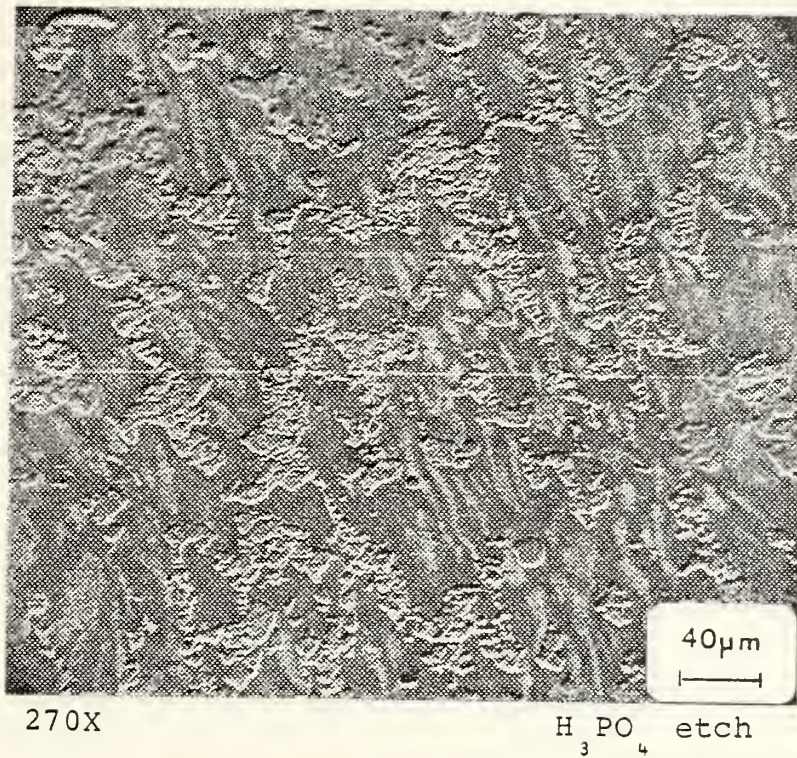
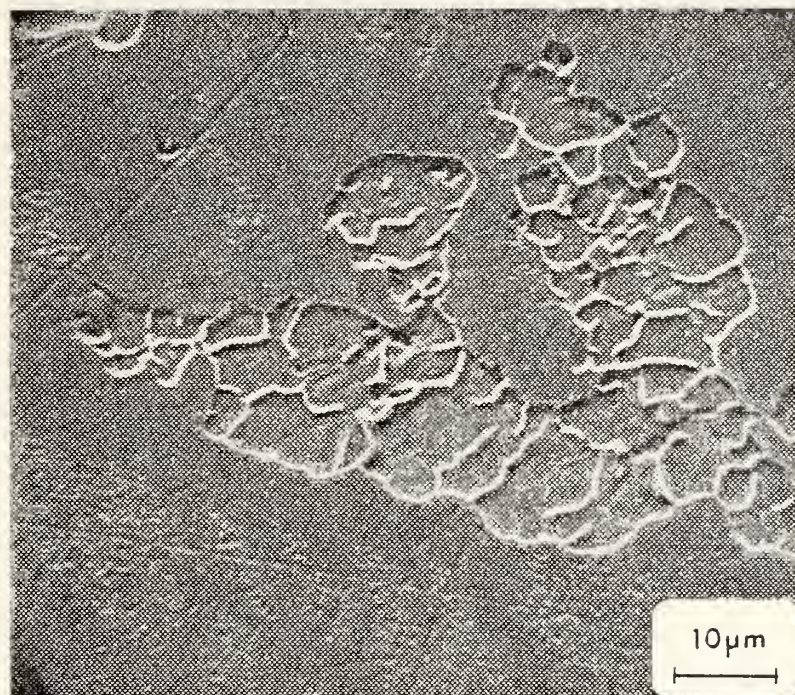


Figure 34 - SEM Photomicrograph of VEX0219-3 (Al-19Mg) showing the results of exposure to six thermal cycles with deformation imposed during the cooling half cycles. The coarse  $\beta$  regions have been fractured and become discontinuous but not eliminated. There is a fine precipitate structure appearing within the Al-Mg solid solution, but it is much less uniform than that created by strictly thermal cycling.







1360X

$\text{H}_3\text{PO}_4$  etch

Figure 35 - SEM photomicrograph of VEX0219-3 (Al-19Mg) showing the result of thermal cycling concurrent with deformation. This coarse  $\beta$  region was continuous in the cast structure but has been fractured, and the Al-Mg matrix has filled the fissures created by working.





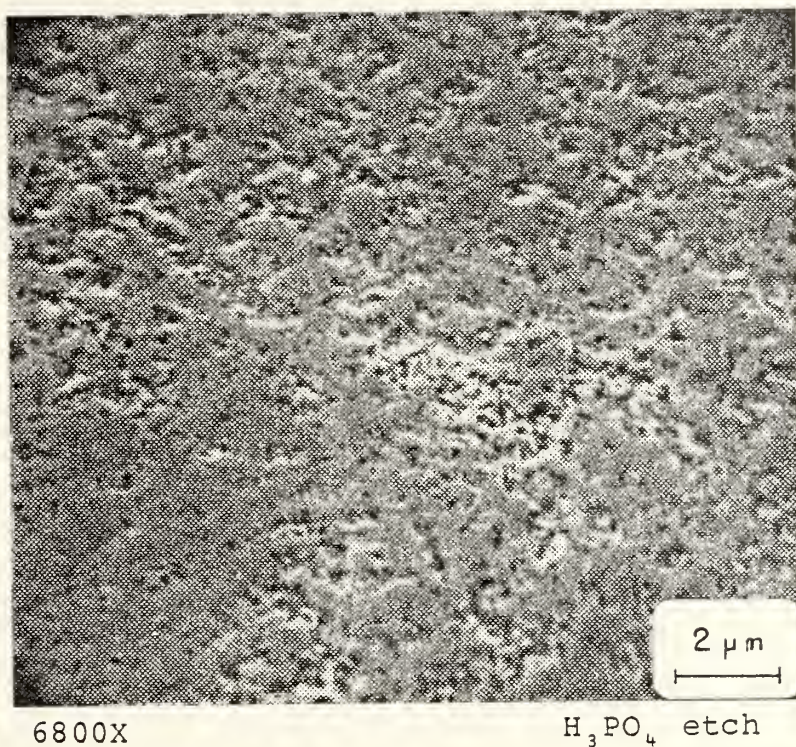


Figure 36 - SEM photomicrograph of VEX0219-3 (Al-19Mg) deformed during thermal cycling. The effect of deformation on the precipitate structure appears to be the creation of more nucleation sites creating a fine, equiaxed structure as opposed to the Widmannstatten structure observed in purely thermal treatments.



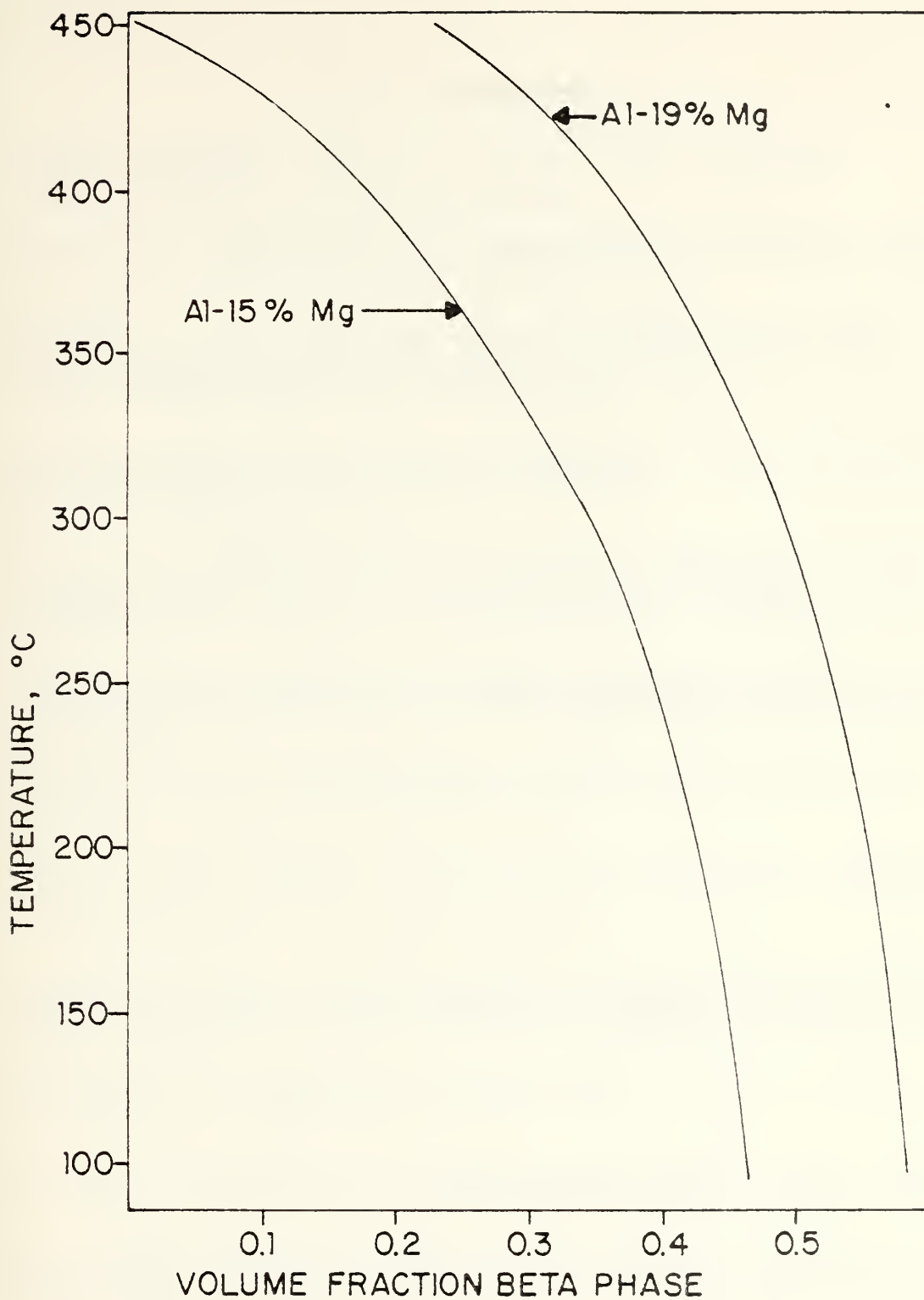


Figure 37 - Graphical illustration of the volume fraction of  $\beta$  phase present in equilibrium microstructures for compositions of 15 and 19 weight percentage Mg in Al.



## LIST OF REFERENCES

1. Metals Handbook, 8th ed., v. 8, pp. 343, 120-129, American Society for Metals, 1973.
2. Hansen, M. and Anderko, K., Constitution of Binary Alloys, 2d ed., pp. 105-109, McGraw-Hill, 1958.
3. Savitsky, E. M., The Influence of Temperature on the Mechanical Properties of Metals and Alloys, pp. 238-252, Stanford University Press, 1962.
4. Brick, R. M., Pense, A. W., and Gordon, R. B., Structure and Properties of Engineering Materials, 4th ed., pp. 95, 251-253, McGraw-Hill, 1977.
5. Ness, F. G., High Strength to Weight Aluminum-18 Weight Percent Magnesium Alloy Through Thermal Mechanical Processing, M.S. Thesis, Naval Postgraduate School, 1976.
6. Glover, T. L., Effects of Thermo-Mechanical Processing on Aluminum-Magnesium Alloys Containing High Weight Percentage Magnesium, M.S. Thesis, Naval Postgraduate School, 1977.
7. Samuels, L. E., Metallographic Polishing by Mechanical Methods, p. 110, Pitman Press, 1967.
8. Alden, T. H., "Review Topics in Superplasticity," Treatise on Materials Science and Technology, v. 6, pp. 234-235, 1975.
9. Cipriani, A. L., An Investigation of the Mechanical Properties of Warm Rolled Aluminum-17.5 Weight Percent Copper Alloy, M.S. Thesis, Naval Postgraduate School, 1976.
10. Dieter, G. E., Mechanical Metallurgy, 2d ed., p. 357, McGraw-Hill, 1976.
11. Guy, A. G. and Hren, J., Elements of Physical Metallurgy, 3rd ed., pp. 228-235, Addison-Wesley, 1974
12. U. S. Naval Weapons Support Center, Materials Analysis and Technology Division, "Report on Aluminum-Magnesium Alloy Trace Element Analysis," MATD-N297, 18 October 1977. 4 pp.
13. Coutu, V. and Krashes, D., "Selecting Chemical Analysis Methods," Metal Progress, v. 112, No. 4, pp. 35-37, September 1977.





# INITIAL DISTRIBUTION LIST

	No. Copies
1. Defense Documentation Center Cameron Station Alexandria, Virginia 22314	2
2. Library, Code 0142 Naval Postgraduate School Monterey, California 93940	2
3. Department Chairman, Code 69 Department of Mechanical Engineering Naval Postgraduate School Monterey, California 93940	1
4. Professor T. R. McNelley, Code 69Mc Department of Mechanical Engineering Naval Postgraduate School Monterey, California 93940	3
5. LT Charles P. Bingay, USN Department of Weapons and Systems Engineering U. S. Naval Academy Annapolis, Maryland 21402	1



Thesis  
B54245  
c.1

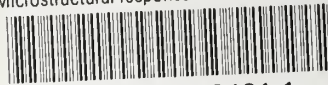
Bingay

172302

Microstructural re-  
sponse of aluminum-  
magnesium alloys to  
thermomechanical proc-  
essing.

thesB54245

Microstructural response of aluminum-mag



3 2768 002 13461 1

DUDLEY KNOX LIBRARY